Probabilistic Engineering Mechanics 24 (2009) 473–492

Contents lists available at ScienceDirect

Probabilistic Engineering Mechanics

journal homepage: www.elsevier.com/locate/probengmech

Experimental case studies for uncertainty quantification in structural dynamics

S. Adhikari [a,*,1], M.I. Friswell [a,2], K. Lonkar [b,3], A. Sarkar [c,4]

[a] School of Engineering, Swansea University, Singleton Park, Swansea SA2 8PP, United Kingdom
[b] Department of Aeronautics and Astronautics Engineering, Stanford University, Stanford, CA, USA
[c] Department of Civil and Environmental Engineering, Carleton University, Ottawa, Canada

ARTICLE INFO

Article history:
Received 20 June 2007
Received in revised form
14 January 2009
Accepted 21 January 2009
Available online 11 February 2009

Keywords:
Experimental modal analysis
Stochastic dynamical systems
Uncertainty quantification
Model validation
Beam experiment

ABSTRACT

The consideration of uncertainties in numerical models to obtain the probabilistic descriptions of vibration response is becoming more desirable for industrial-scale finite element models. Broadly speaking, there are two aspects to this problem. The first is the quantification of parametric and non-parametric uncertainties associated with the model and the second is the propagation of uncertainties through the model. While the methods of uncertainty propagation have been extensively researched in the past three decades (e.g., the stochastic finite element method), only relatively recently has quantification been considered seriously. This paper considers uncertainty quantification with the aim of gaining more insight into the nature of uncertainties in medium- and high-frequency vibration problems. This paper describes the setup and results from two experimental studies that may be used for this purpose. The first experimental work described in this paper uses a fixed–fixed beam with 12 masses placed at random locations. The total 'random mass' is about 2% of the total mass of the beam and this experiment simulates 'random errors' in the mass matrix. The second experiment involves a cantilever plate with 10 randomly placed spring-mass oscillators. The oscillating mass of each of the 10 oscillators is about 1% of the mass of the plate. One hundred nominally identical dynamical systems are created and individually tested for each experiment. The probabilistic characteristics of the frequency response functions are discussed in the low, medium and high frequency ranges. The variability in the amplitude of the measured frequency response functions is compared with numerical Monte Carlo simulation results. The data obtained in these experiments may be useful for the validation of uncertainty quantification and propagation methods in structural dynamics.

1. Introduction

Finite element codes implementing physics-based models are used extensively for the dynamic analysis of complex systems. Laboratory-based controlled tests are often performed to gain insight into some specific physical aspects of a problem. Such tests can indeed lead to new physical laws improving the computational models. Test data can also be used to calibrate a known model. However, neither of these activities may be enough to produce a credible numerical tool because of several types of uncertainties which exist in the physics-based computational framework. Such uncertainties include, but are not limited to (a) parameter uncertainty (e.g, uncertainty in geometric parameters, friction coefficient, strength of the materials involved); (b) model uncertainty (arising from the lack of scientific knowledge about the model which is *a priori* unknown); (c) experimental error (uncertain and unknown errors percolate into the model when they are calibrated against experimental results). These uncertainties must be assessed and managed for credible computational predictions.

The predictions from high resolution numerical models may sometimes exhibit significant differences with the results from physical experiments due to uncertainty. When substantial statistical information exists, the theory of probability and stochastic processes offer a rich mathematical framework to represent such uncertainties. In a probabilistic setting, the data (parameter) uncertainty associated with the system parameters, such as the geometric properties and constitutive relations (i.e. Young's

* Corresponding author. Tel.: + 44 (0) 1792 602088; fax: + 44 (0) 1792 295676.
E-mail addresses: S.Adhikari@swansea.ac.uk (S. Adhikari), M.I.Friswell@swansea.ac.uk (M.I. Friswell), kuldeep@stanford.edu (K. Lonkar), abhijit_sarkar@carleton.ca (A. Sarkar).
URLs: http://engweb.swan.ac.uk/~adhikaris (S. Adhikari), http://michael.friswell.com (M.I. Friswell), http://structure.stanford.edu/People/phDstudents/kuldeep/kuldeep.htm (K. Lonkar), http://www.abhijitsarkar.net/ (A. Sarkar).
1 Chair of Aerospace Engineering.
2 Professor of Aerospace Structures.
3 Graduate Student.
4 Assistant Professor and Canada Research Chair.

0266-8920/$ – see front matter © 2009 Elsevier Ltd. All rights reserved.
doi:10.1016/j.probengmech.2009.01.005

modulus, mass density, Poisson's ratio, damping coefficients), can be modelled as random variables or stochastic processes using the so-called parametric approach. These uncertainties can be quantified and propagated, for example, using the stochastic finite element method [1–14].

Recently, the uncertainty due to modelling error has received attention as this is crucial for model validation [15–23]. The model uncertainty problem poses serious challenges as the parameters contributing to the modelling errors are not available *a priori* and therefore precludes the application of a parametric approach to address such issues. Model uncertainties do not explicitly depend on the system parameters. For example, there can be unquantified errors associated with the equation of motion (linear or non-linear), in the damping model (viscous or non-viscous [24,25]), in the model of structural joints. The model uncertainty may be tackled by the so-called non-parametric method pioneered by Soize [26–28] and adopted by others [29–34].

Uncertainties associated with a variable can be characterised using the probabilistic approach or possibilistic approaches based on interval algebra, convex sets or Fuzzy sets. In this paper the probabilistic approach has been adopted. The equation of motion of a damped n-degree-of-freedom linear structural dynamic system can be expressed as

$$\mathbf{M}\ddot{\mathbf{q}}(t) + \mathbf{C}\dot{\mathbf{q}}(t) + \mathbf{K}\mathbf{q}(t) = \mathbf{f}(t) \tag{1}$$

where $\mathbf{M} \in \mathbb{R}_{n,n}$, $\mathbf{C} \in \mathbb{R}_{n,n}$ and $\mathbf{K} \in \mathbb{R}_{n,n}$ are the mass, damping and stiffness matrices respectively. The importance of considering parametric and/or non-parametric uncertainty also depends on the frequency of excitation. For example, in high-frequency vibration the wavelengths of the vibration modes become very small. As a result the vibration response can be very sensitive to the small details of the system. In general, three different approaches are currently available to analyse stochastic structural dynamic systems across the frequency range:

- *Low-frequency vibration problems*: Stochastic Finite Element Method [1–14] (SFEM)—considers parametric uncertainties in detail;
- *High frequency vibration problems*: Statistical Energy Analysis [35–37] (SEA)—does not consider parametric uncertainties in detail;
- *Mid-frequency vibration problems* [38–42]: both parametric and non-parametric uncertainties need to be considered.

The majority of the studies reported in probabilistic mechanics are based on analytical or simulation methods. Often simulation based methods are used to validate approximate but relatively fast prediction tools (such as perturbation-based methods). Experimental results are rare because of difficulties such as (a) generating nominally identical samples of a structural system, (b) the resources and effort involved in testing a large number of samples, (c) the repetitive nature of the experimental procedure and (d) ensuring that different samples are tested in exactly the same way so that no uncertainty arises due to the measurement process. In spite of these difficulties some authors have conducted experimental investigations on random dynamical systems. For structure-borne noise, Kompella and Bernhard [43] measured 57 frequency response functions at driver microphones for different pickup trucks. Fahy [44, page 275] reported measurements of FRFs on 41 nominally identical beer cans. Both of these experiments show variability in nominally identical engineered systems. Friswell et al. [45] reported two experiments where random systems were 'created' in the laboratory for the purpose of model validation. The first experiment used a randomly moving mass on a free-free beam and the second experiment involved a copper pipe with uncertain internal pressure. Fifty nominally identical random samples were created and tested for both experiments.

Table 1
Material and geometric properties of the beam considered for the experiment.

Beam properties	Numerical values
Length (L)	1200 mm
Width (b)	40.06 mm
Thickness (t_h)	2.05 mm
Mass density (ρ)	7800 kg/m^3
Young's modulus (E)	2.0×10^5 MPa
Cross sectional area ($a = bt_h$)	8.212×10^{-5} m^2
Moment of inertia ($I = 1/12bt_h^3$)	2.876×10^{-11} m^4
Mass per unit length (ρ_l)	0.641 kg/m
Bending rigidity (EI)	5.752 N m^2
Total weight	0.7687 kg

This paper describes two experimental studies that may be used to test methods of uncertainty quantification across the frequency range. The tests are closely controlled and the uncertainty can be considered to be 'known' for all practical purposes. This allows one to model uncertainty, propagate it through dynamical models and compare the results with this experimentally obtained data. The first experiment described in this paper uses a fixed–fixed beam with 12 masses placed at random locations. The total *random mass* is about 2% of the total mass of the beam and this experiment simulates *random errors* in the mass matrix. One hundred nominally identical dynamical systems are created and individually tested in the Bristol Laboratory for Advanced Dynamic Engineering (BLADE). The model of the beam and experimental setup are described in Section 2.1. The experimental method to test one hundred nominally identical structures is discussed in Section 2.2. In Section 2.3 the probabilistic characteristics of the amplitude of the measured frequency response functions are discussed in the low, medium and high frequency ranges. In Section 2.4 the experimental system with random mass distribution is numerically simulated using Euler–Bernoulli beam theory and Monte Carlo simulation. In Section 2.5 the mean and standard deviation of the amplitude of the experimentally measured frequency response functions are compared with Monte Carlo simulation results. The model of the cantilever plate and the experimental setup are described in Section 3.1. The experimental method to test one hundred nominally identical systems is discussed in Section 3.2. In Section 3.3 the probabilistic characteristics of the amplitude of the measured frequency response functions are discussed in the low-, medium- and high-frequency ranges. In Section 3.4 the experimental system with random mass distribution is numerically simulated using the thin plate theory and Monte Carlo simulation. In Section 3.5 the mean and standard deviation of the amplitude of the experimentally measured frequency response functions are compared with Monte Carlo simulation results. The key results and the contributions of this work are discussed Section 4. The data presented here are available on the world wide web for research purposes. The web address is http://engweb.swan.ac.uk/~adhikaris/uq/. This data may be used to validate different uncertainty quantification and propagation methods in structural dynamics.

2. The beam experiment

2.1. System model and experimental setup

A steel beam with uniform rectangular cross-section is used for the experiment. The physical and geometrical properties of the steel beam are shown in Table 1.

The beam is actually a 1.5 m long ruler made of steel. The use of a ruler ensures that the masses may be easily placed at predetermined locations. The ruler is clamped between 0.05 m and 1.25 m so that the effective length of the vibrating beam is 1.2 m. The overall experimental setup is shown in Fig. 1.

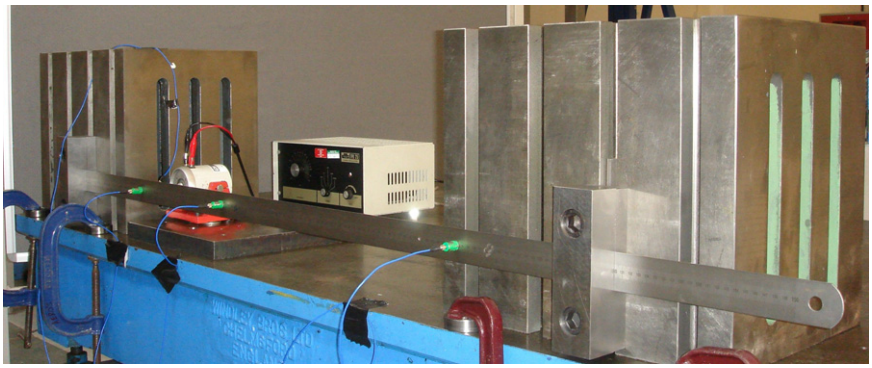

Fig. 1. The test rig for the fixed–fixed beam.

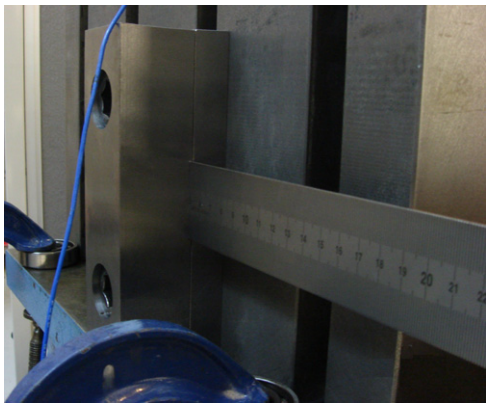

(a) Left end.

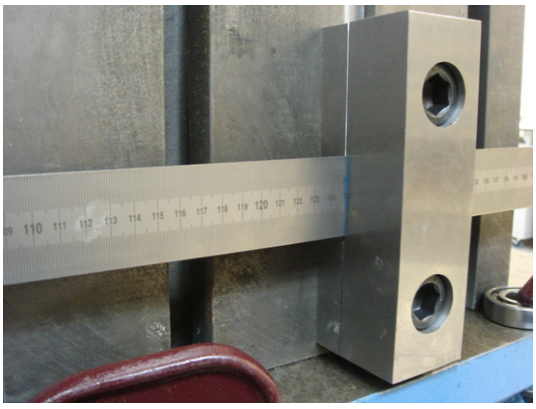

(b) Right end.

Fig. 2. The clamping arrangements at the two ends of the beam. The clamping arrangement is aimed at providing fixed–fixed boundary conditions.

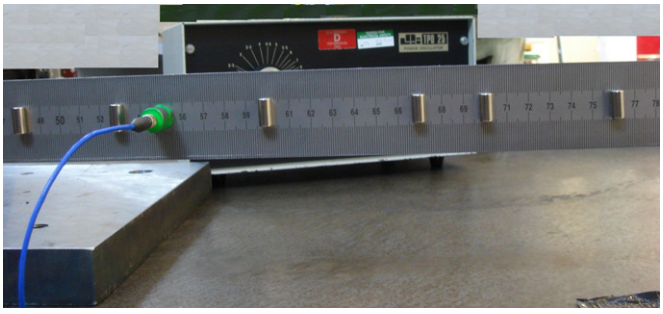

Fig. 3. The attached masses (magnets) at random locations. In total 12 masses, each weighting 2 g, are used.

The end clamps are bolted to two heavy steel blocks, which in turn are fixed to a rigid table with bolts as shown in Fig. 2. The clamping arrangements are aimed at providing fixed–fixed boundary conditions.

The edges of both the solid metal blocks are sharpened to ensure that no rotation is allowed beyond the 'true end' of the beam. It should be emphasised that it is, in general, extremely difficult to ensure there is no residual stress in a clamped or any other constrained system. Due to the fixed nature of the supports and flexibility of the beam, our initial tests show that the beam was in compression and was buckling in the first mode (the first natural frequency turned out to be close to zero and significantly lower than predicted by the Euler–Bernoulli beam theory). The length between the supports was adjusted to minimise the compression or tension in the beam. Because the supports were not disturbed during the entire test spanning 100 realisations, we expect that the residual stress did not change from sample to sample.

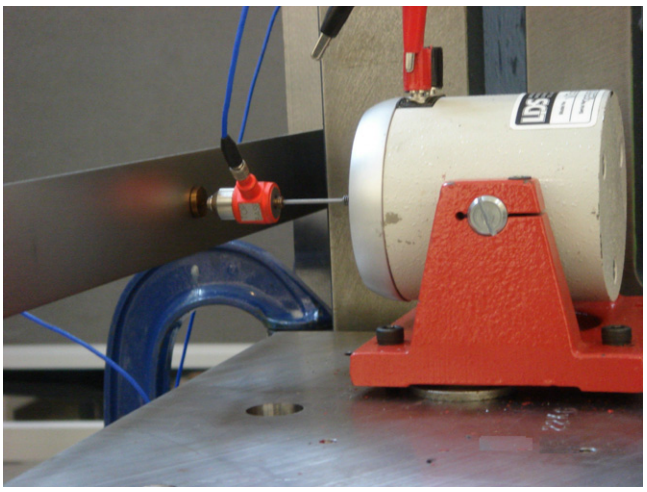

Fig. 4. The shaker is used as an impulse hammer which in turn is controlled via Simulink™ and dSpace™. A hard steel tip was used and small brass plate weighting 2 g is attached to the beam to take the impact from the shaker.

Twelve equal masses are used to simulate a randomly varying mass distribution. The masses are actually magnets so that they can be easily attached at any location on the steel beam. These magnets are cylindrical in shape, with a length of 12.0 mm and a diameter of 6.0 mm. Some of the attached masses for a sample realisation are shown in Fig. 3.

Each mass weighs 2 g so that the total variable mass is 1.6% of the mass of the beam. The location of the 12 masses are assumed to be between 0.2 m and 1.0 m from the left end of the beam. A uniform distribution with 100 samples is used to generate the

Table 2
The details of the accelerometers and the force transducer for the beam experiment.

Role	Model & Serial number	Position from the left end	Channel	Sensitivity
Sensor (accelerometer)	PCB 333M07 SN 25948	23 cm (Point 1)	1	98.8 mV/g
Sensor (accelerometer)	PCB 333M07 SN 26018	50 cm (Point 2)	2	101.2 mV/g
Sensor (accelerometer)	PCB 333M07 SN 25942	102 cm (Point 3)	3	97.6 mV/g
Actuator (force transducer)	PCB 208C03 21487	50 cm (Point 2)	4	2.24 mV/N

mass locations. The mean and the standard deviations of the mass locations are given by

$$\bar{\mathbf{x}}_m = [0.2709, 0.3390, 0.3972, 0.4590, 0.5215, 0.5769, 0.6398, 0.6979, 0.7544, 0.8140, 0.8757, 0.9387]\ \text{m} \quad (2)$$

and

$$\sigma_{\mathbf{x}_m} = [0.0571, 0.0906, 0.1043, 0.1034, 0.1073, 0.1030, 0.1029, 0.1021, 0.0917, 0.0837, 0.0699, 0.0530]\ \text{m}. \quad (3)$$

2.2. Experimental methodology

Experimental modal analysis [46–48] is used in this work. The three main components of the implemented experimental technique are (a) the excitation of the structure, (b) the sensing of the response, and (c) the data acquisition and processing. In this experiment a shaker was used (the make, model no. and serial no. are LDS, V201, and 92358.3, respectively) to act as an impulse hammer. The usual manual impact hammer was not used because of the difficulty in ensuring the impact occurs at exactly at the same location with the same force for every sample run. The shaker generates impulses at a pulse interval of 20 s and a pulse width of 0.01 s. Using the shaker in this way eliminates, as far as possible, any uncertainties arising from the input forces. This innovative experimental technique is designed to ensure that the resulting uncertainty in the response arises purely due to the random locations of the attached masses. Fig. 4 shows the arrangement of the shaker.

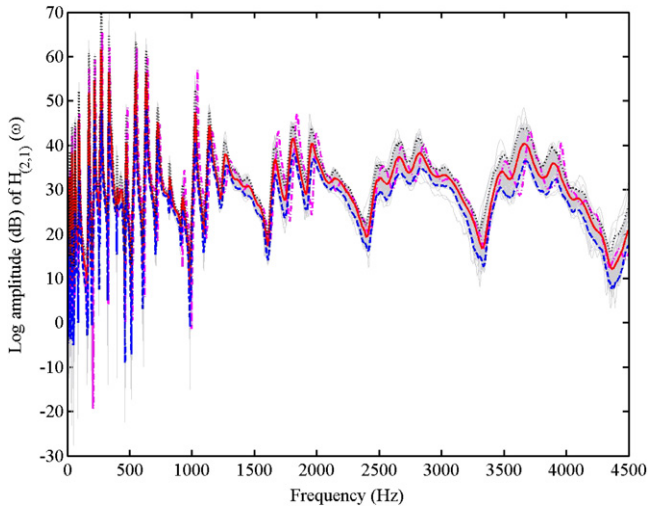

(a) Response across the frequency range.

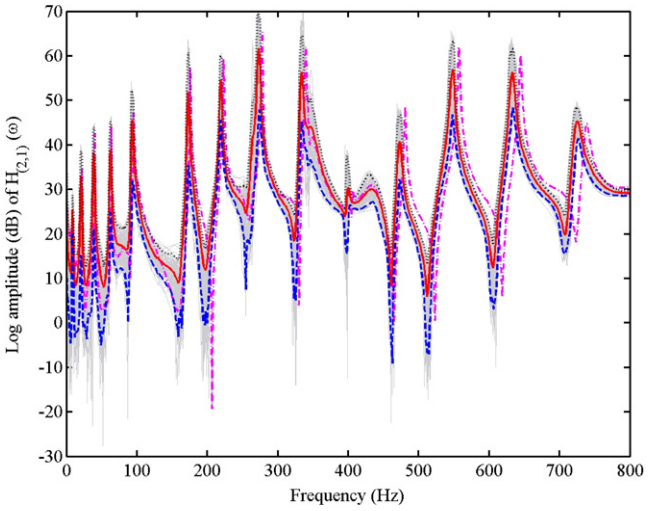

(b) Low-frequency response.

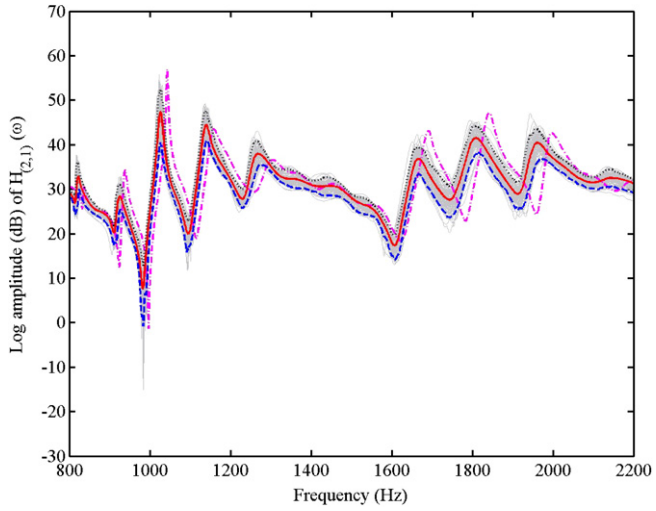

(c) Medium-frequency response.

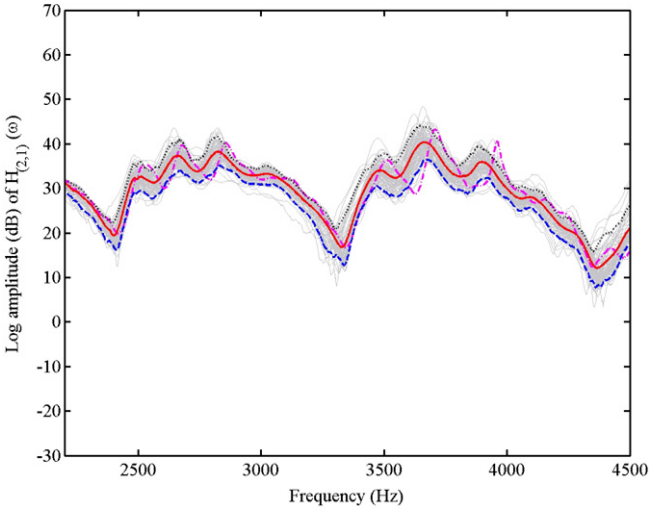

(d) High-frequency response.

Fig. 5. Experimentally measured amplitude of the FRF of the beam at point 1 (23 cm from the left end) with 12 randomly placed masses. 100 random FRFs, together with the FRF of the baseline system (- -) ensemble mean (-), 5% (-.-) and 95% (...) probability lines are shown.

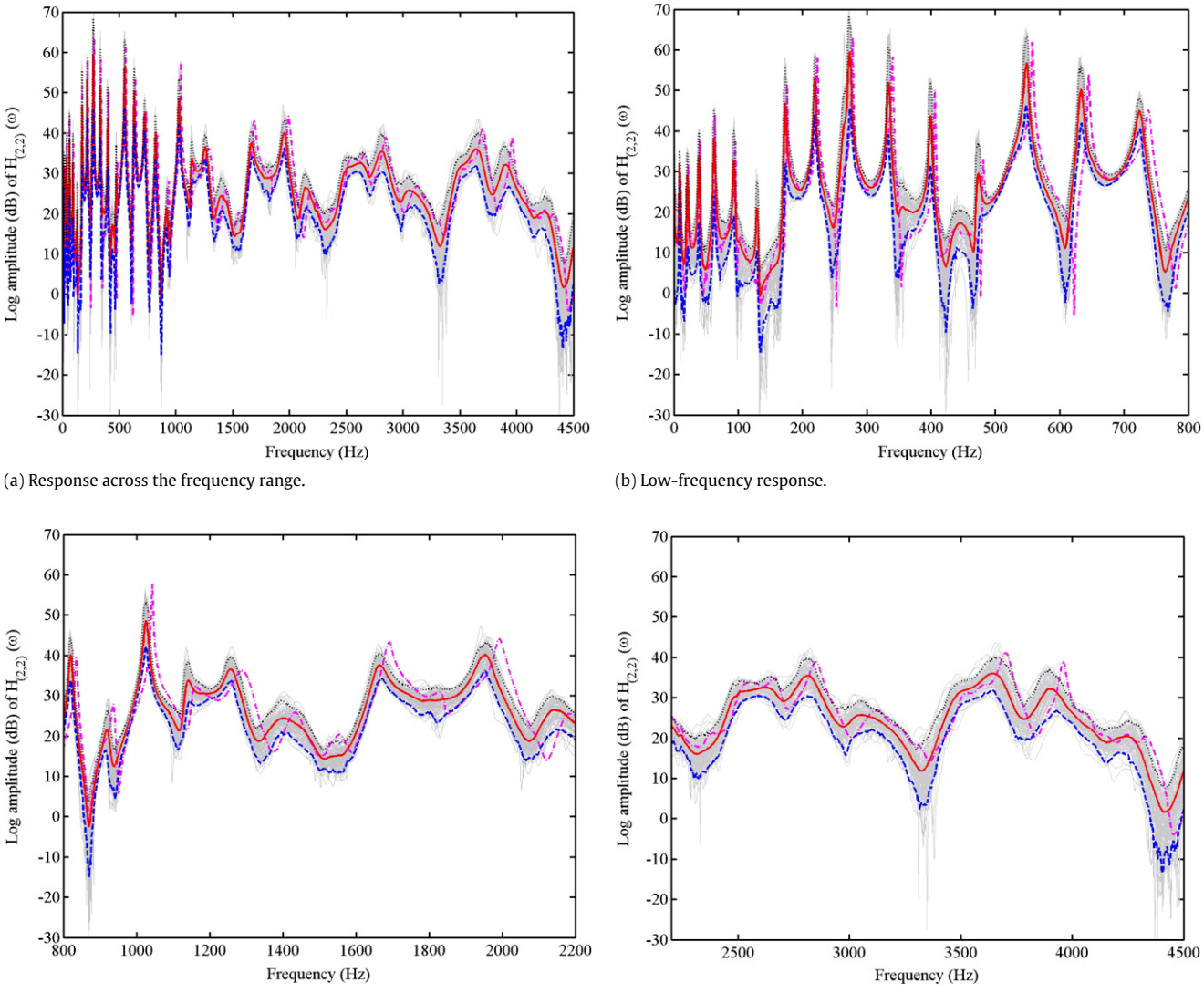

(a) Response across the frequency range.

(b) Low-frequency response.

(c) Medium-frequency response.

(d) High-frequency response.

Fig. 6. Experimentally measured amplitude of the FRF of the beam at point 2 (the driving-point FRF, 50 cm from the left end) with 12 randomly placed masses. 100 random FRFs, together with the FRF of the baseline system (- -) ensemble mean (-), 5% (-.-) and 95% (...) probability lines are shown.

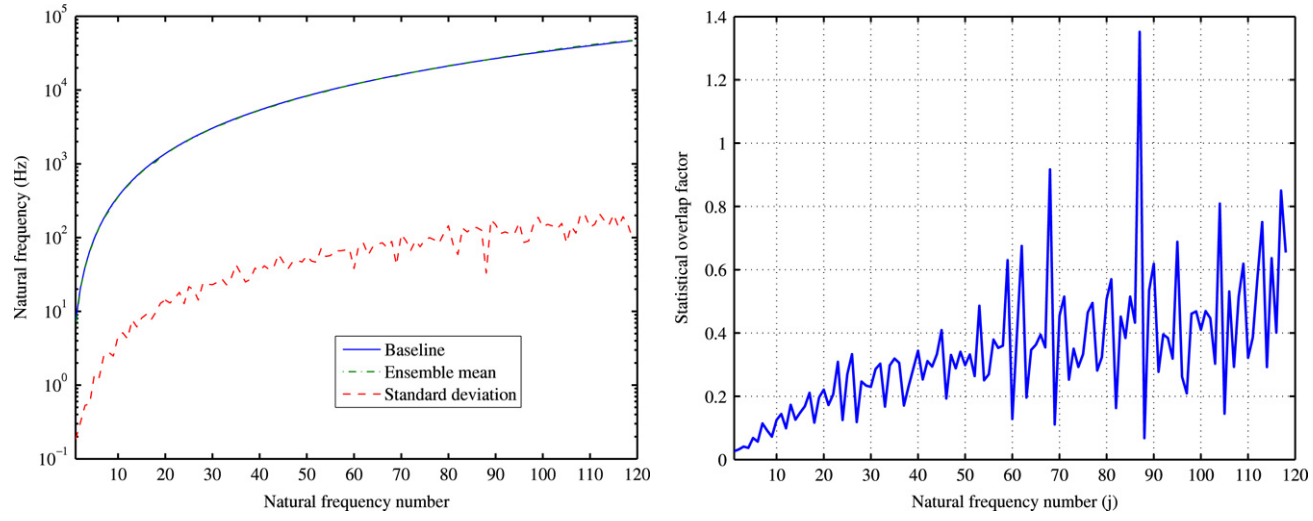

(a) Natural frequency statistics.

(b) Statistical overlap factors.

Fig. 7. Mean, standard deviation and statistical overlap factor of the natural frequencies of the beam with random mass.

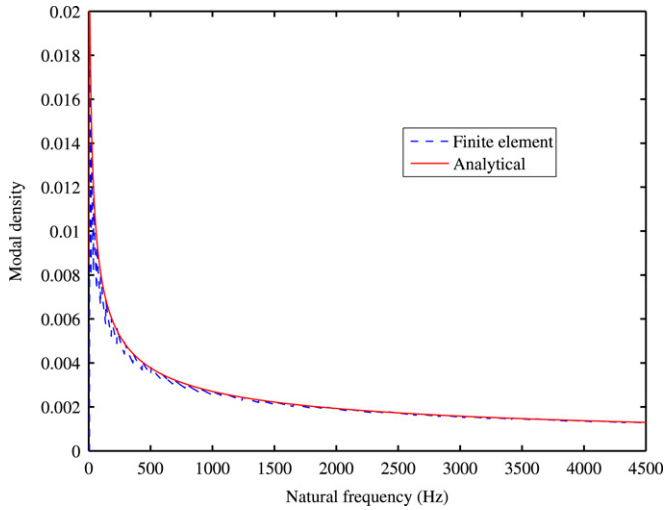

(a) Modal densities ($\nu(\omega)$) of the baseline beam obtained using the analytical expression and finite element method.

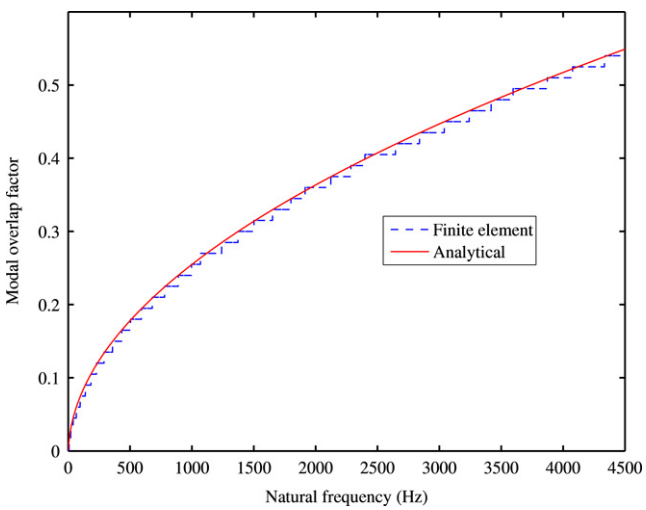

(b) Modal overlap factors of the baseline beam obtained using the analytical expression and finite element method.

Fig. 8. The variation of the modal densities and modal overlap factors of the baseline system with respect to driving frequency.

A hard steel tip is used for the hammer to increase the frequency range of excitation. The beam material was relatively 'soft' compared to the hard steel tip, resulting in indentation marks. To avoid this problem a small circular brass plate of mass 2 g is attached to the beam to take the impact from the shaker. The details of the force transducer attached to the shaker is given in Table 2.

In this experiment three accelerometers are used as the response sensors. The locations of the three sensors are selected such that two of them are near the two ends of the beam and one is at the exciter location, near the middle of the beam, so that driving-point frequency response function may be obtained. The exact locations are calculated such that the nodal lines of the first few bending modes are avoided. The details of the accelerometers, including their locations, are shown in Table 2.

Small holes are drilled into the beam and the three accelerometers are attached by bolts through these holes.

The signal from the force transducer is amplified using a KISTLER type 5134 amplifier (with settings Gain: 100, Filter: 10K and Bias: Off) while the signals from the accelerometers are directly input into a 32 channel LMS^{TM} system. For data acquisition and processing, LMS Test Lab 5.0 is used. In Impact Scope, the bandwidth is set to 8192 Hz with 8192 spectral lines (i.e., 1.00 Hz resolution). The steel tip used in the experiment only gives clean data up to approximately 4500 Hz, and thus 4500 Hz is used as the upper limit of the frequency in the measured frequency response functions. The data logged beyond 4500 Hz should be ignored.

2.3. Results and discussions

We will discuss results corresponding to point 1 (a cross FRF) and point 2 (the driving-point FRF) only. Results for the other point are not shown to save space but can be obtained from the uploaded data file. Fig. 5 shows the amplitude of the frequency response function (FRF) at point 1 (see Table 2 for the location) of the beam without any masses (the baseline model). In the same figure 100 samples of the amplitude of the FRF are shown together with the ensemble mean, 5% and 95% probability lines.

Fig. 5(b)–(d) show the low-, medium- and high-frequency response separately, obtained by zooming around the appropriate frequency ranges in Fig. 5(a). There are, of course, no fixed and definite boundaries between the low-, medium- and high-frequency ranges. Here we have selected 0–0.8 kHz as the low-frequency vibration, 0.8–2.2 kHz as the medium-frequency vibration and 2.2–4.5 kHz as the high-frequency vibration. The modal overlap factors corresponding to these frequency ranges will be discussed later in Section 2.4. These frequency boundaries are selected on the basis of the qualitative nature of the response and devised purely for the presentation of the results. The experimental approach discussed here is independent of these selections. The ensemble mean follows the result of the baseline system closely only in the low-frequency range. In the higher modes, the mean natural frequencies are lower than the baseline system. This is because the mass of the baseline system is lower than the random system realisations. The relative variability of the amplitude of the FRF remains more or less constant in the mid- and high-frequency ranges. Equivalent results for point 2 (the driving-point FRF, see Table 2 for the location) are shown in Fig. 6.

The general trend of the results is similar to that of point 1. The measured FRF data up to 4.5 kHz as shown here is significantly noise-free, since the hard steel tip used was able to excite the whole frequency range. The experimental data shown throughout the paper is the 'raw data' (that is, without any filtering) obtained directly from the LMS system.

2.4. Numerical simulation

In this section we model the beam and the attached masses at random locations using a Monte Carlo simulation. As shown in Fig. 1, the beam is uniform and clamped at both ends. We include the 12 randomly located masses, the mass of the three accelerometers (6 g each) and the mass of the small circular brass plate (2 g) to take the impact from the impulse hammer. The equation of motion of the undamped 'mass loaded beam' can be expressed as

$$EI\frac{\partial^4 w(x,t)}{\partial x^4} + m\ddot{w}(x,t) + \sum_{j=1}^{12} m_r \ddot{w}(x_{r_j},t) + \sum_{j=1}^{3} m_a \ddot{w}(x_{a_j},t) + m_b \ddot{w}(x_b,t) = f(x,t) \tag{4}$$

where EI is the bending stiffness of the beam, x is the spatial coordinate along the length of the beam, t is the time, $w(x,t)$ is the time dependent transverse deflection of the beam, $f(x,t)$ is the applied time depended load on the beam, m is the mass per unit length of the beam and L is the length of the beam.

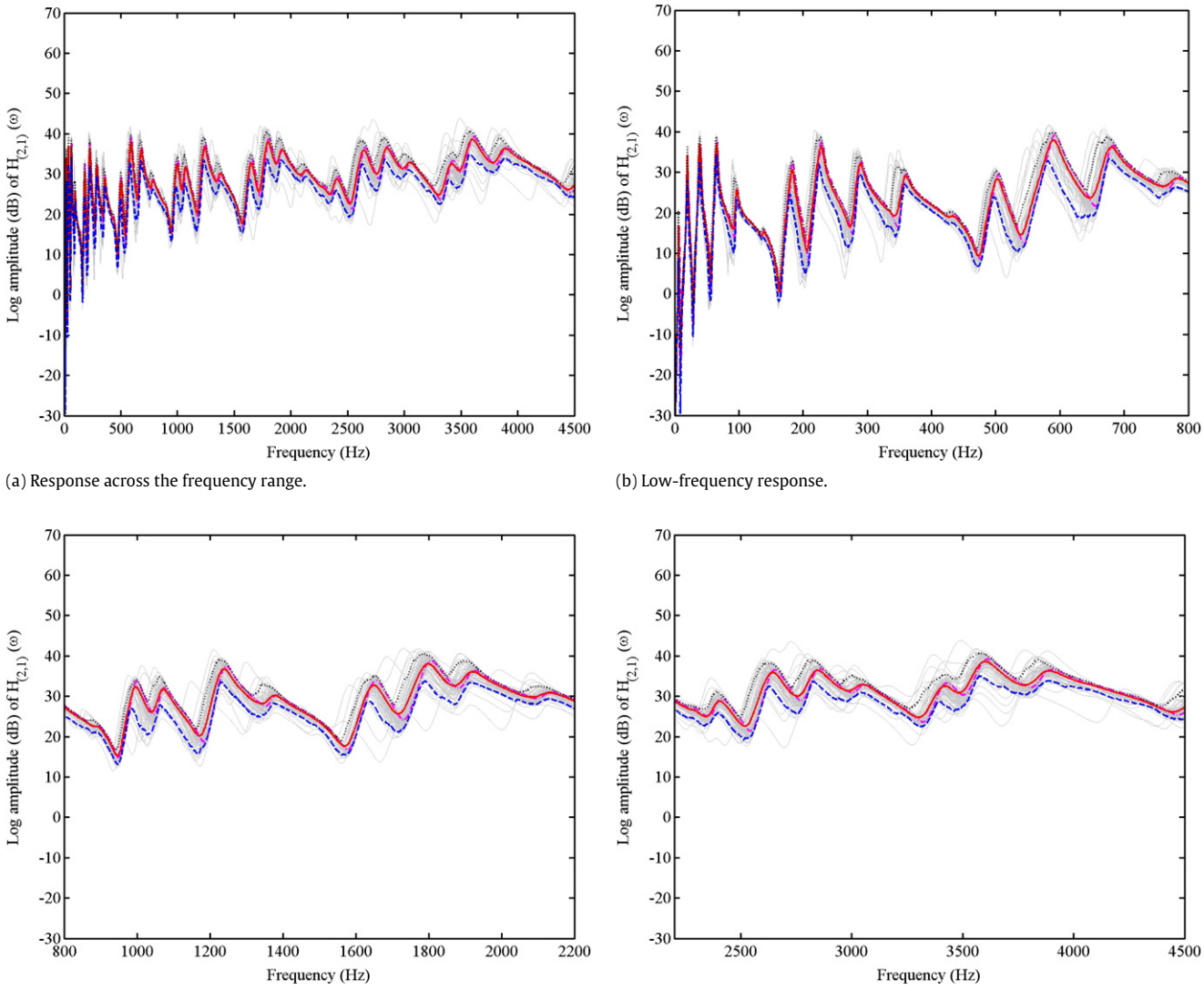

(a) Response across the frequency range.

(b) Low-frequency response.

(c) Medium-frequency response.

(d) High-frequency response.

Fig. 9. Numerically calculated amplitude of the FRF of the beam at point 1 (23 cm from the left end) with 12 randomly-placed masses. 100 random FRFs, together with the FRF of the baseline system (- -) ensemble mean (-), 5% (-.-) and 95% (...) probability lines are shown.

Due to the impulse input at location x_b, the applied force has the mathematical form

$$f(x,t) = \delta(t)\delta(x - x_b) \tag{5}$$

where $\delta(\bullet)$ is the Dirac delta function. The damping of the system is introduced using the constant modal damping assumption. Here m_r is the added mass at random locations x_{r_j} on the beam, m_a is the mass of an accelerometer placed at locations x_{a_j} and m_b is the mass of the circular brass plate located at x_b. Due to the randomness in x_{r_j}, Eq. (4) becomes a random partial differential equation. The nth natural frequency of the baseline beam [49] is given by

$$\omega_n \approx \frac{(2n+1)^2\pi^2}{4L^2}\sqrt{\frac{EI}{m}}, \quad n = 1, 2, \ldots, n. \tag{6}$$

For the random system, an in-house finite element code was developed to implement the discretised version of Eq. (4). The natural frequencies of the baseline beam, together with the mean and standard deviation of the natural frequencies of the random system is shown in Fig. 7(a).

The natural frequencies of linear systems with uncertain parameters can be obtained by solving random eigenvalue problems (see for example [50,51]). An intuitive way to quantify uncertainty in linear dynamical systems is to use the statistical overlap factor, [52], defined as the ratio of the standard deviation of the natural frequencies to the average spacing of the natural frequencies. Fig. 7(b) shows the statistical overlap factors of the natural frequencies of the beam obtained using Monte Carlo simulation. From Fig. 7(a) observe that the standard deviation of the natural frequencies are quite small compared to the mean values. This is also reflected in Fig. 7(b) where it can be observed that, on average, the statistical overlap factors of the system is below 0.5. This implies that we do not expect significant mid-frequency or high-frequency type of behaviour. Experimental

Table 3
Material and geometric properties of the cantilever plate considered for the experiment.

Plate properties	Numerical values
Length (L_x)	998 mm
Width (L_y)	530 mm
Thickness (t_h)	3.0 mm
Mass density (ρ)	7860 kg/m^3
Young's modulus (E)	2.0×10^5 MPa
Poisson's ratio (μ)	0.3
Total weight	12.47 kg

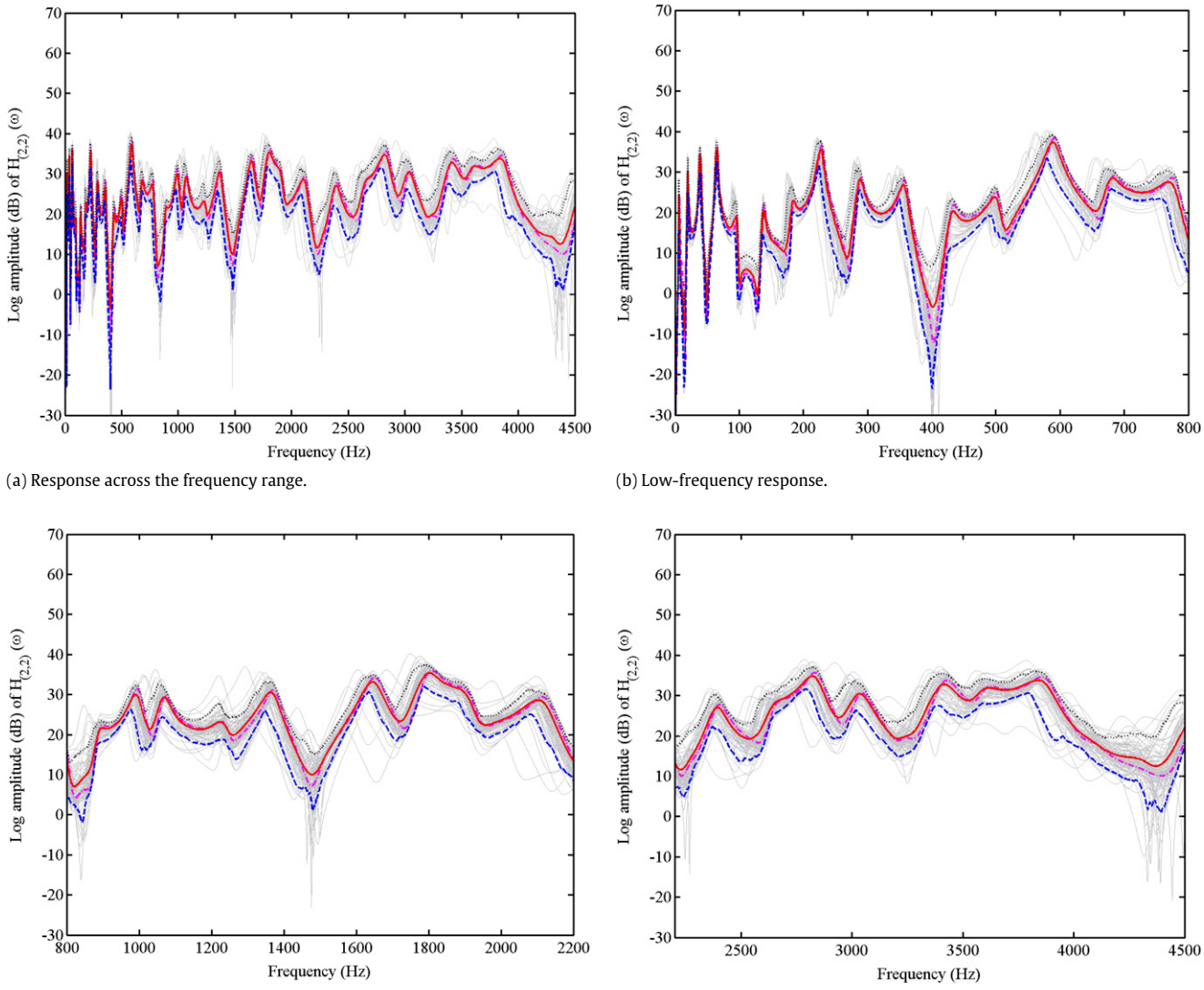

(a) Response across the frequency range.

(b) Low-frequency response.

(c) Medium-frequency response.

(d) High-frequency response.

Fig. 10. Numerically calculated amplitude of the FRF of the beam at point 2 (the driving-point FRF, 50 cm from the left end) with 12 randomly placed masses. 100 random FRFs, together with the FRF of the baseline system (- -) ensemble mean (-), 5% (-.-) and 95% (...) probability lines are shown.

Table 4
Stiffnesses of the springs and natural frequencies of the oscillators used to simulate unmodelled dynamics (the mass of the each oscillator is 121.4 g).

Oscillator number	Spring stiffness ($\times 10^4$ N/m)	Natural frequency (Hz)
1	1.6800	59.2060
2	0.9100	43.5744
3	1.7030	59.6099
4	2.4000	70.7647
5	1.5670	57.1801
6	2.2880	69.0938
7	1.7030	59.6099
8	2.2880	69.0938
9	2.1360	66.7592
10	1.9800	64.2752

results shown in Figs. 5 and 6 support this conclusion. We have calculated modal densities and modal overlap factors of the baseline system using the finite element approach and analytical expression given by Xie et al. [53]. The modal density ν for the fixed–fixed beam can be obtained as

$$\nu(\omega) = \frac{L}{\pi}\left(\frac{m}{EI}\right)^{1/4}\omega^{-1/2} - \frac{1}{2}\omega^{-1}. \tag{7}$$

The variation of the modal densities obtained from the above equation and finite element method is shown in Fig. 8(a).

Assuming a constant modal damping factor ζ, the modal overlap factor of the system can be calculated as

$$\mu(\omega) = \omega\zeta\nu(\omega) = \zeta\frac{L}{\pi}\left(\frac{m}{EI}\right)^{1/4}\omega^{1/2} - \frac{\zeta}{2}. \tag{8}$$

Using $\zeta = 0.015$, the variation of the modal overlap factors obtained from the above equation and finite element method is shown in Fig. 8(b). This result shows that the modal overlap factor is below 0.2 in the low frequency range (0–0.8 kHz), it is below 0.4 in the mid-frequency range (0.8–2.2 kHz) and it is over 0.4 in the high-frequency range (2.2–4.5 kHz) considered. Again we stress that these boundaries are introduced purely for the purpose of presentation of the experimental results.

The frequency response function of the system between points x_0 and x is calculated using the modal superposition and assuming proportional damping as

$$H(\omega, x_0, x) = \sum_n \frac{\phi_n(x)\phi_n(x_0)}{\omega_n^2 - \omega^2 + 2\mathrm{i}\zeta_n\omega\omega_n}. \tag{9}$$

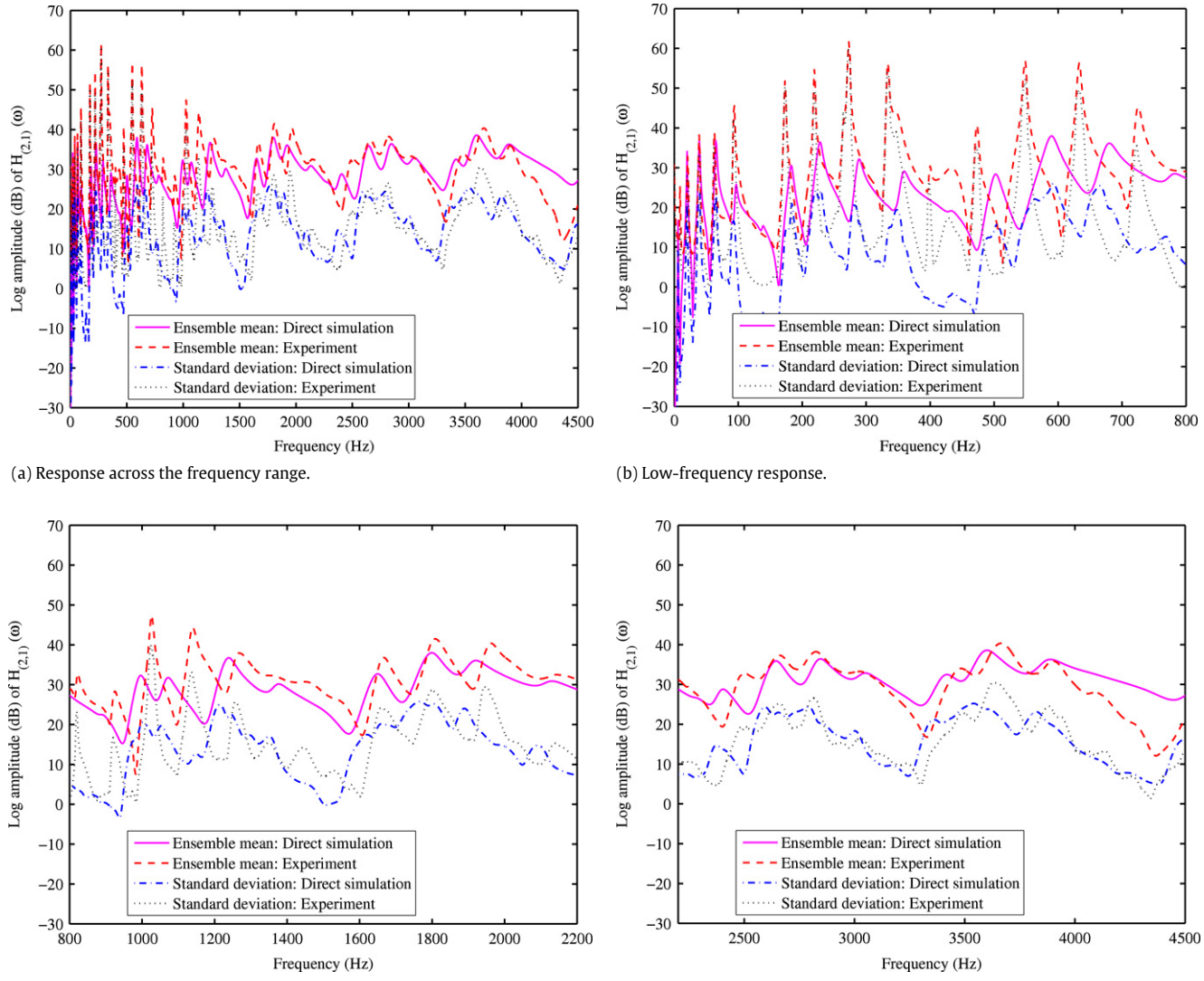

(a) Response across the frequency range.

(b) Low-frequency response.

(c) Medium-frequency response.

(d) High-frequency response.

Fig. 11. Comparison of the mean and standard deviation of the amplitude of the beam at point 1 (23 cm from the left end) using direct Monte Carlo simulation and experiment.

Here $\phi_n(x)$ is the nth mode shape (normalized to unit modal mass) and ζ_n is the damping factor for the nth mode and $x_0 = 0.50$ m is the location of the shaker input point. We calculate the output at two points for $x = 0.50$ m and $x = 0.23$ m. In the numerical calculations 120 elements are used and the resulting finite element model has 238 degrees of freedom. Half of the modes, that is 119 modes, are used in the calculation of the frequency response function in Eq. (9). A constant modal damping factor of 1.5% (that is $\zeta_n = 0.015$) is assumed for all of the modes.

The location of 100 sets of mass positions used for the experiment is again used for the Monte Carlo simulation. Fig. 9 shows the amplitude of the frequency response function (FRF) at point 1 (see Table 2 for the location) of the beam without any masses (the baseline model). In the same figure 100 samples of the amplitude of the FRF are shown together with the ensemble mean, 5% and 95% probability lines. Fig. 9(b)–(d) show the low-, medium- and high-frequency response separately, obtained by zooming around the appropriate frequency ranges in Fig. 9(a). Equivalent results for point 2 (the driving-point FRF, see Table 2 for the location) are shown in Fig. 10. For both the points, the ensemble mean follows the result of the baseline system fairly closely over the entire frequency range. This is somewhat different from that observed in the experimental results. The relative variance of the amplitude of the FRF remains more or less constant in the mid- and high-frequency ranges, which is qualitatively similar to the experimental results.

2.5. Comparisons between numerical and experimental results

In this section we compare the experimental results with the Monte Carlo simulation results. Fig. 11 compares the ensemble mean and standard deviation of the amplitude of the frequency response function (FRF) at point 1 obtained from the experiment and Monte Carlo simulation. Fig. 11(b)–(d) show the low-, medium- and high-frequency response separately, obtained by zooming around the appropriate frequency ranges in Fig. 11(a). Direct comparisons between experimental and simulation results for stochastic dynamical systems have not been widely reported in the literature. The standard deviation of the amplitude of the FRF reaches a peak at the system natural frequencies, which is also predicted by the numerical simulation. Qualitatively the simulation results agree well with the experimental results. The main reason for the discrepancies, especially in the low-frequency regions, is probably due to the incorrect value of the damping factors. In the simulation study a constant damping factor of 1.5% is assumed for all of the modes. Ideally one should measure modal

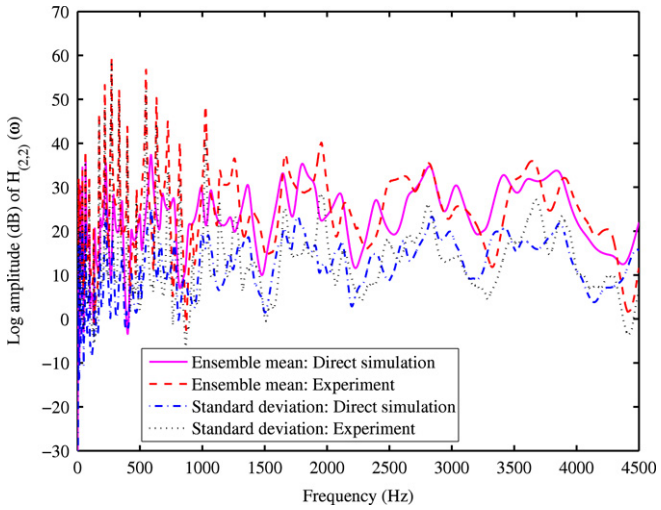

(a) Response across the frequency range.

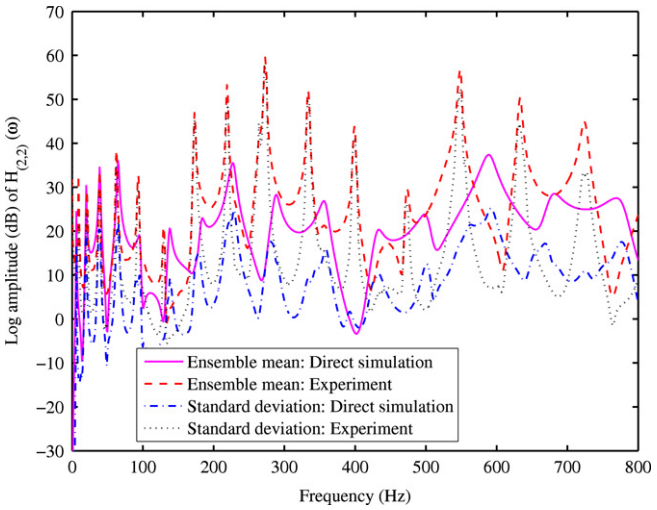

(b) Low-frequency response.

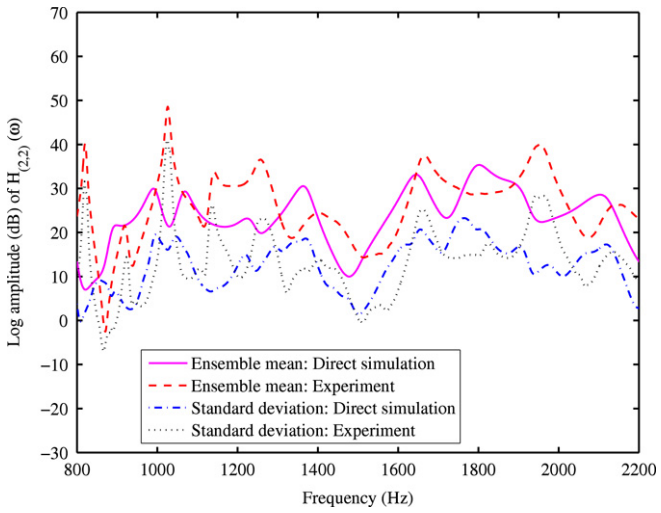

(c) Medium-frequency response.

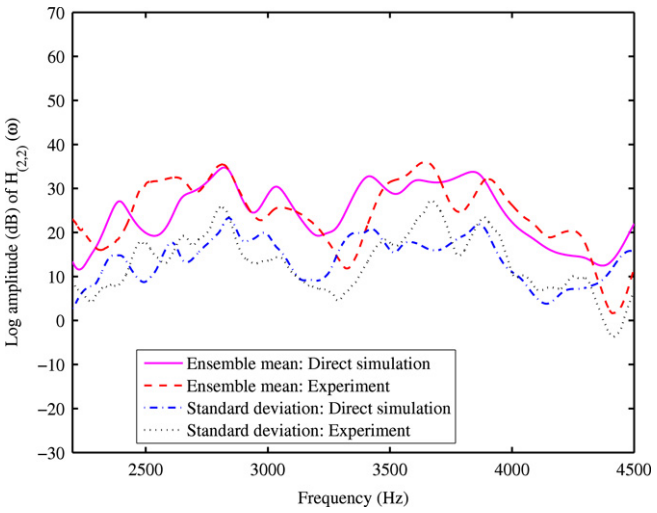

(d) High-frequency response.

Fig. 12. Comparison of the mean and standard deviation of the amplitude of the beam at point 2 (the driving-point FRF, 50 cm from the left end) using direct Monte Carlo simulation and experiment.

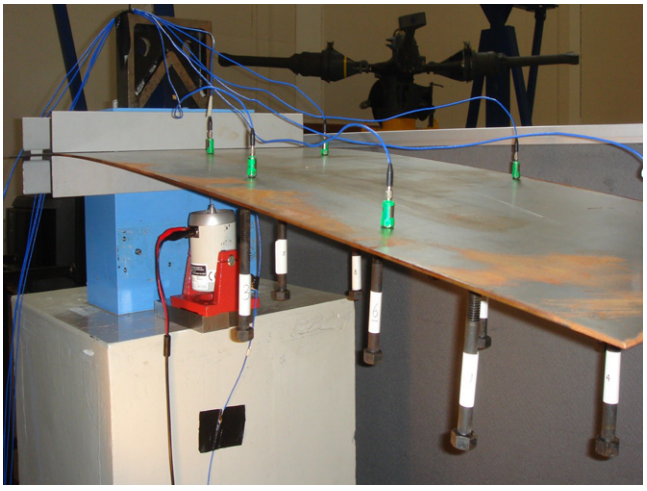

(a) Front view of the experimental setup.

(b) Side view of the experimental setup.

Fig. 13. The test rig for the cantilever plate.

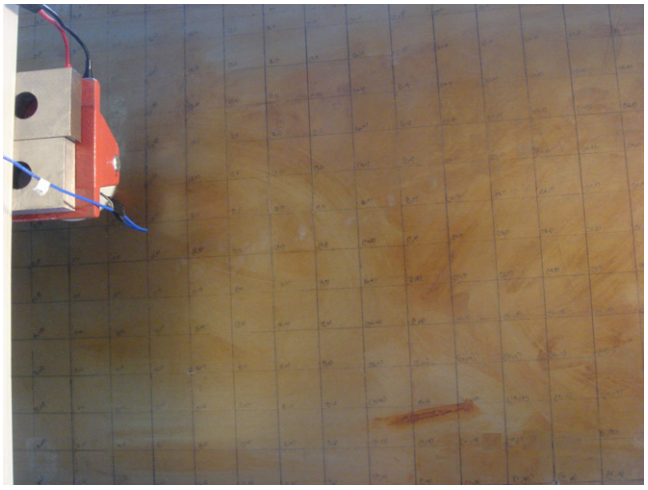

Fig. 14. Grid numbering strategy on the bottom surface of the plate to attach the oscillators.

Fig. 15. Details of a typical oscillator used to simulate unmodelled dynamics. Fixed mass (magnet) 2 g, oscillatory mass (the bolt) 121.4 g. The oscillatory mass is about 1% of the total mass of the plate. The spring stiffness varies between 1.5 and 2.4×10^4 N/m.

damping factors from experimental measurements for all of the samples and for as many modes as possible and perhaps take an average across the samples for every mode. Such an average will only give good predictions when the modal overlap factor is high.

Equivalent comparisons for point 2 (the driving-point FRF) are shown in Fig. 12. For both points, the experimental mean and standard deviation in the low-frequency range is quite high compared to numerical results. This can again be attributed to the wrong values of modal damping factors in the analytical model since the pattern of the peaks are strikingly similar but they are separated in 'height'. This is a clear indication that the damping values are incorrect in the simulation model. Therefore, one of the key outcomes of this experimental study is that wrong values of the modal damping factors can lead to significant errors in the response variance prediction even if everything else is performed correctly.

A constant modal damping factor assumption is often used for dynamic analysis of many practical systems. This is often one of the main choices to include damping offered by many commercial

Fig. 16. Attached oscillators at random locations. The spring stiffness varies so that the oscillator frequencies are between 43 and 70 Hz.

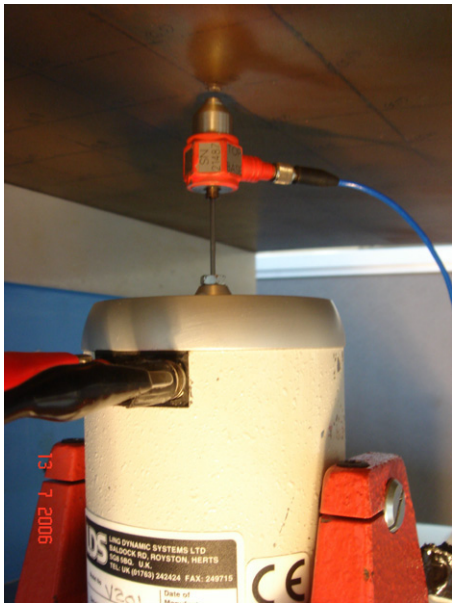

Fig. 17. The shaker used to provide an impulse excitation using Simulink™ and dSpace™. A hard steel tip was used and the shaker was placed at node (4, 6).

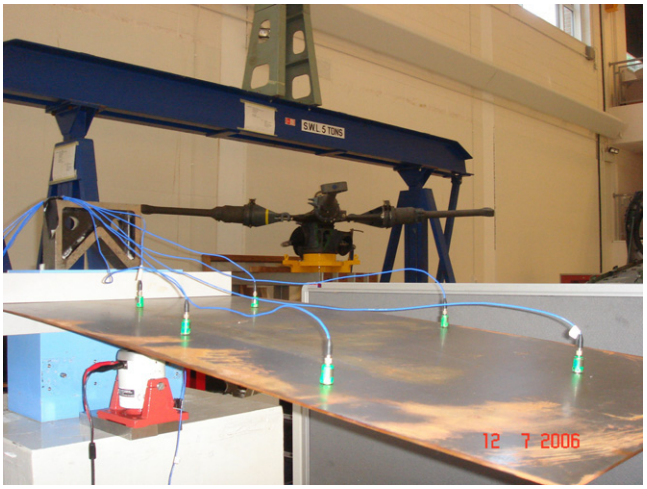

Fig. 18. The positions of the accelerometers on the plate.

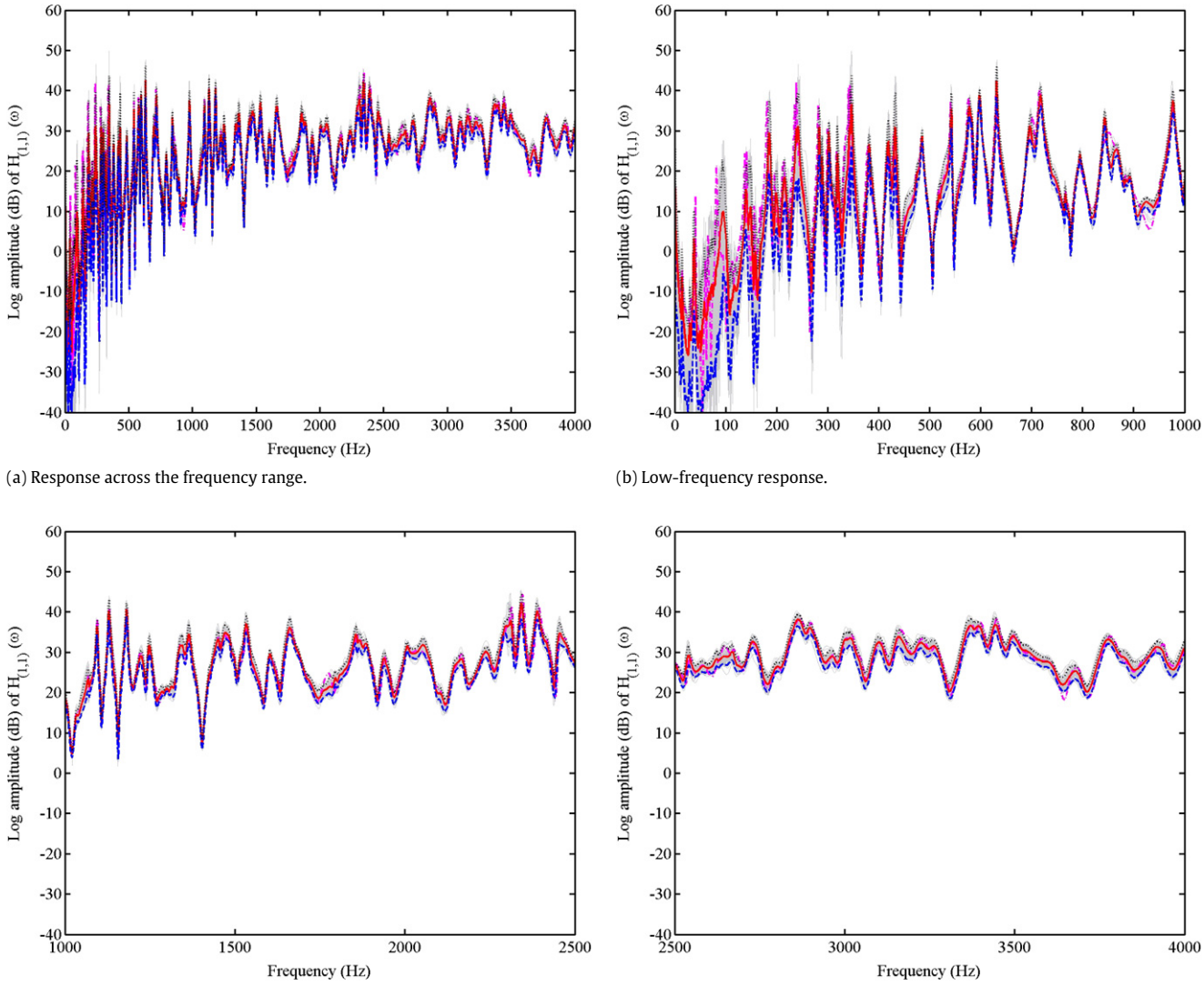

(a) Response across the frequency range.

(b) Low-frequency response.

(c) Medium-frequency response.

(d) High-frequency response.

Fig. 19. Experimentally measured amplitude of the driving-point FRF of the plate at point 1 (nodal coordinate: (4, 6)) with 10 randomly placed oscillators. 100 random FRFs, together with the FRF of the baseline system (- -) ensemble mean (-), 5% (-.-) and 95% (...) probability lines are shown.

Table 5
The details of the six accelerometers attached to the top of the plate.

Model & Serial number	Coordinates	LMS channel	Sensitivity (mV/g)
333M07 SN 25948	Point 1: (4, 6)	1	98.8
333M07 SN 26254	Point 2: (6, 11)	2	96.7
333M07 SN 26018	Point 3: (11, 3)	3	101.2
333M07 SN 25942	Point 4: (14, 14)	4	97.6
333M07 SN 26280	Point 5: (18, 2)	5	101.3
333M07 SN 26016	Point 6: (21, 10)	6	100.0

finite element and structural analysis packages. Furthermore, high-frequency vibration analysis methods such as the Statistical Energy Analysis (SEA) [35] uses the constant loss factor assumption for all modes. Our experimental results highlight a possible shortcoming of this simplified approach in the context of probabilistic structural dynamics. Since the peaks are fairly 'clean', in theory one can identify individual modal damping factors for all possible modes corresponding to all of the 100 measured FRFs. This approach might lead to a better overall agreement between the theory and experimental results. However, care must be taken so that each experimental mode is correctly paired with each theoretical mode to ensure that the damping is added to the correct modes in the model. With a relatively small number of measured degrees of freedom, this task can be difficult and might lead to further modelling error.

3. The plate experiment

3.1. System model and experimental setup

The aim of the experiment is to simulate the influence of uncertain subsystems on the dynamics of a plate. The uncertain dynamics is realised by 10 spring-mass oscillators with randomly distributed stiffness properties attached at random locations. This test rig, as with the previous experiment described before, has been

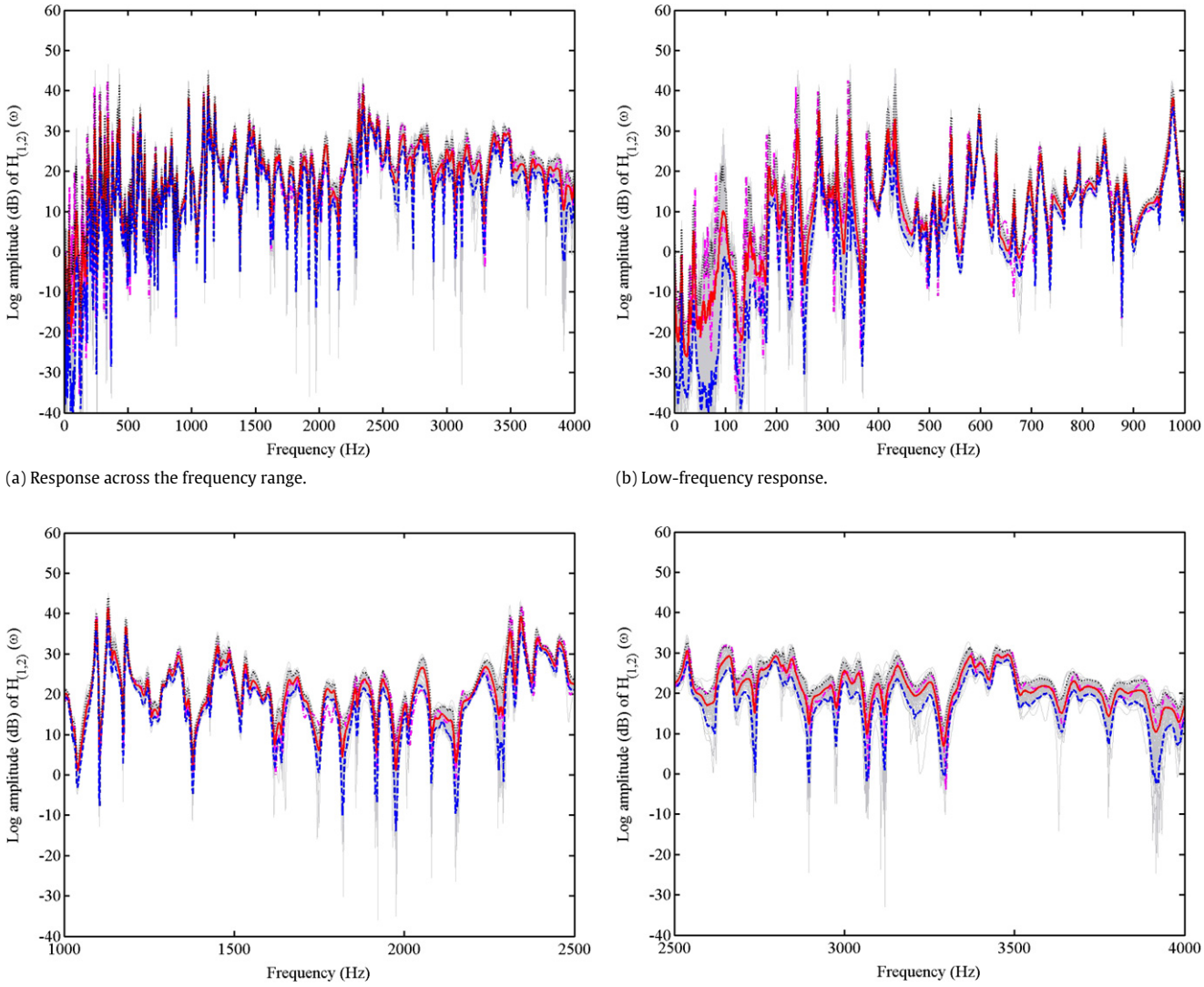

(a) Response across the frequency range.

(b) Low-frequency response.

(c) Medium-frequency response.

(d) High-frequency response.

Fig. 20. Experimentally measured amplitude of the cross-FRF of the plate at point 2 (nodal coordinate: (6,11)) with 10 randomly placed oscillators. 100 random FRFs, together with the FRF of the baseline system (- -) ensemble mean (-), 5% (-.-) and 95% (...) probability lines are shown.

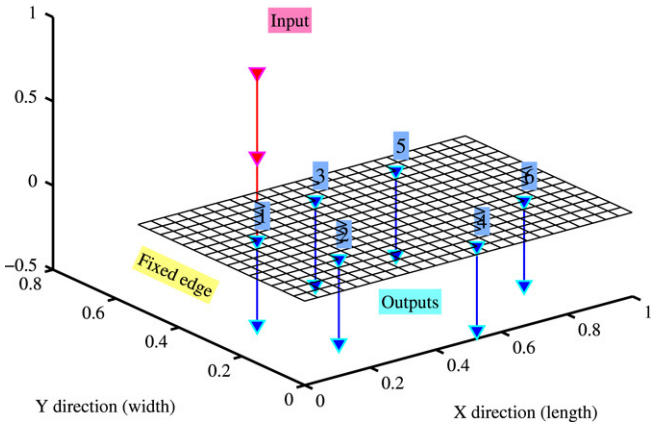

Fig. 21. The Finite Element (FE) model of a steel cantilever plate. The material and geometric properties are: $E = 200 \times 10^9$ N/m^2, $\mu = 0.3$, $\rho = 7860$ kg/m^3, $t_h = 3.0$ mm, $L_x = 0.998$ m, $L_y = 0.53$ m. A 0.7% modal damping is assumed for all modes.

designed for simplicity and ease of replication and modelling. The overall arrangement of the test-rig is shown in Fig. 13.

A rectangular steel plate with uniform thickness is used for the experiment. The physical and geometrical properties of the steel plate are shown in Table 3.

The plate is clamped along one edge using a clamping device. The clamping device is attached to the top of a heavy concrete block and the whole assembly is placed on a steel table. The plate has a mass of approximately 12.47 kg and special care has been taken to ensure its stability and to minimise vibration transmission. The plate is 'divided' into 375 elements (25 along the length and 15 along the width). Taking one corner of the cantilevered edge as the origin, co-ordinates have been assigned to all of the nodes. Oscillators and accelerometers are attached to these nodes. This approach allows easy correlation to a finite element model, where the oscillators are attached and the measurements are made at the nodes of the model. The bottom surface of the plate is marked with the node numbers so that the oscillators can be hung at the nodal locations. The grid numbering scheme is shown Fig. 14. This scheme also reduces the uncertainty arising from the measurement of the locations of the oscillators.

A discrete random number generator is used to generate the X and Y coordinates for the attachment of the oscillators. In total 10

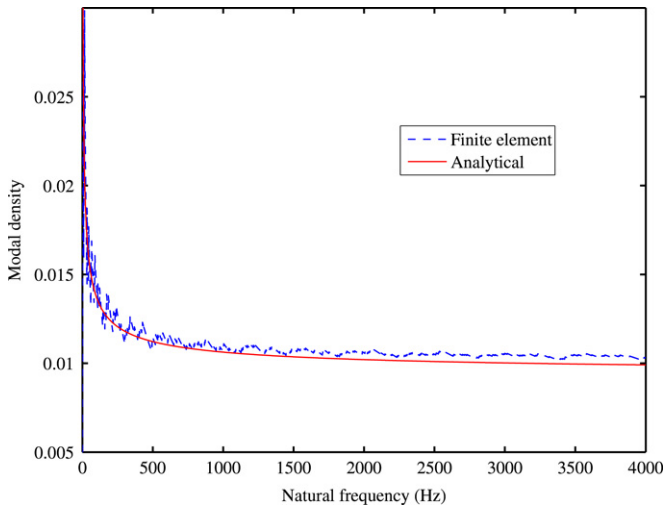

(a) Modal densities ($\nu(\omega)$) of the baseline plate obtained using the analytical expression and finite element method.

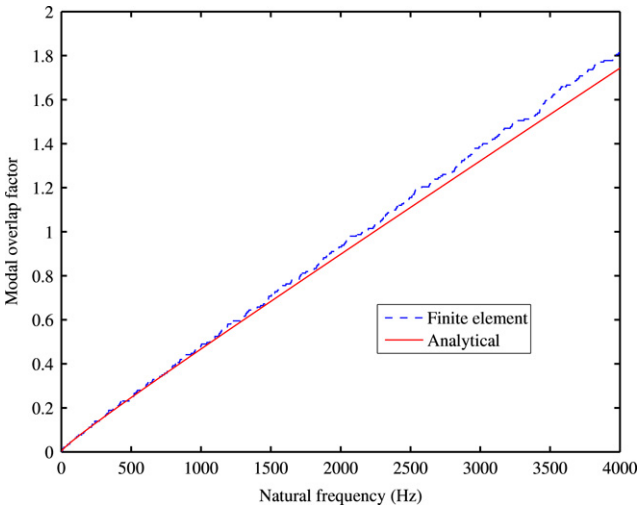

(b) Modal overlap factors of the baseline plate obtained using the analytical expression and finite element method.

Fig. 22. The variation of the modal densities and modal overlap factors of the baseline system with respect to driving frequency.

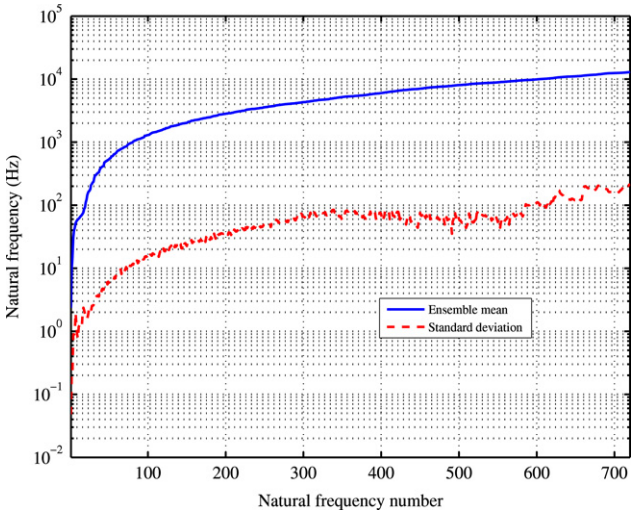

Fig. 23. Mean and standard deviation of the natural frequencies of the plate with randomly placed oscillators.

oscillators are used to simulate uncertain subsystems. The details of a typical oscillator is shown in Fig. 15.

The springs are adhesively bonded to a magnet at the top and a mass at the bottom. The magnet at the top of the assembly allows the oscillators to be easily attached to the bottom of the plate. It should be noted that the mass of the magnets would have the 'fixed mass effect' considered in the previous case study on the beam. However, since the plate is much heavier (≈12.5 kg) than the magnets, the effect of the fixed masses (20 g in total) is negligible. The stiffness values of the 10 springs used in the experiments are given in Table 4. This table also shows the natural frequency of the individual oscillators.

The oscillating mass of each of the 10 oscillators is 121.4 g, and hence the total oscillator mass is 1.214 kg, which is 9.8% of the mass of the plate. The springs are attached to the plate at the pre-generated nodal locations using the small magnets located at the top the oscillator assembly. The small magnets (weighting 2 g) are found to be strong enough to hold the 121.4 g mass attached to the spring below over the frequency range considered. A sample realisation of the attached oscillators is shown in Fig. 16.

One hundred such realisations of the oscillators are created by hanging the oscillators at random locations and are individually tested in this experiment.

3.2. Experimental methodology

The 32-channel LMS^{TM} system and the shaker used in the beam experiment is again employed to perform the modal analysis [46–48]. Fig. 17 shows the arrangement of the shaker.

The shaker was placed so that it impacted at the (4, 6) node of the plate. The shaker was driven by a signal from a Simulink^{TM} and dSpace^{TM} system via a power amplifier (TPO 25 AEI 00051).

In this experiment six accelerometers are used as the response sensors. The locations of the six sensors are selected such that they cover a broad area of the plate. The locations of the accelerometers are shown in Fig. 18.

The details of the accelerometers, including their nodal locations, are shown in Table 5.

Small holes are drilled into the plate and all of the six accelerometers are attached by bolts through the holes. In this experiment 4000 Hz was used as the upper limit of the frequency in the measured frequency response functions.

3.3. Results and discussions

In this paper we will discuss the results corresponding to point 1 (the driving-point FRF) and point 2 (a cross FRF) only. Results for the other four points are not shown to save space but can be obtained from the data file uploaded in world wide web. Fig. 19 shows the amplitude of the frequency response function (FRF) at point 1 (see Table 5 for the location) of the plate without any oscillators (the baseline model). In the same figure 100 samples of the amplitude of the FRF are shown together with the ensemble mean, 5% and 95% probability lines.

In Fig. 19(b)–(d) we have separately shown the low-, medium- and high-frequency response, obtained by zooming around the appropriate frequency ranges in Fig. 19(a). There are, of course, no fixed and definite boundaries between the low-, medium- and high-frequency ranges. Here we have selected 0–1.0 kHz as the low-frequency vibration, 1.0–2.5 kHz as the medium-frequency vibration and 2.5–4 kHz as the high-frequency vibration. The modal overlap factors corresponding to these frequency ranges will be discussed later in Section 3.4. These frequency

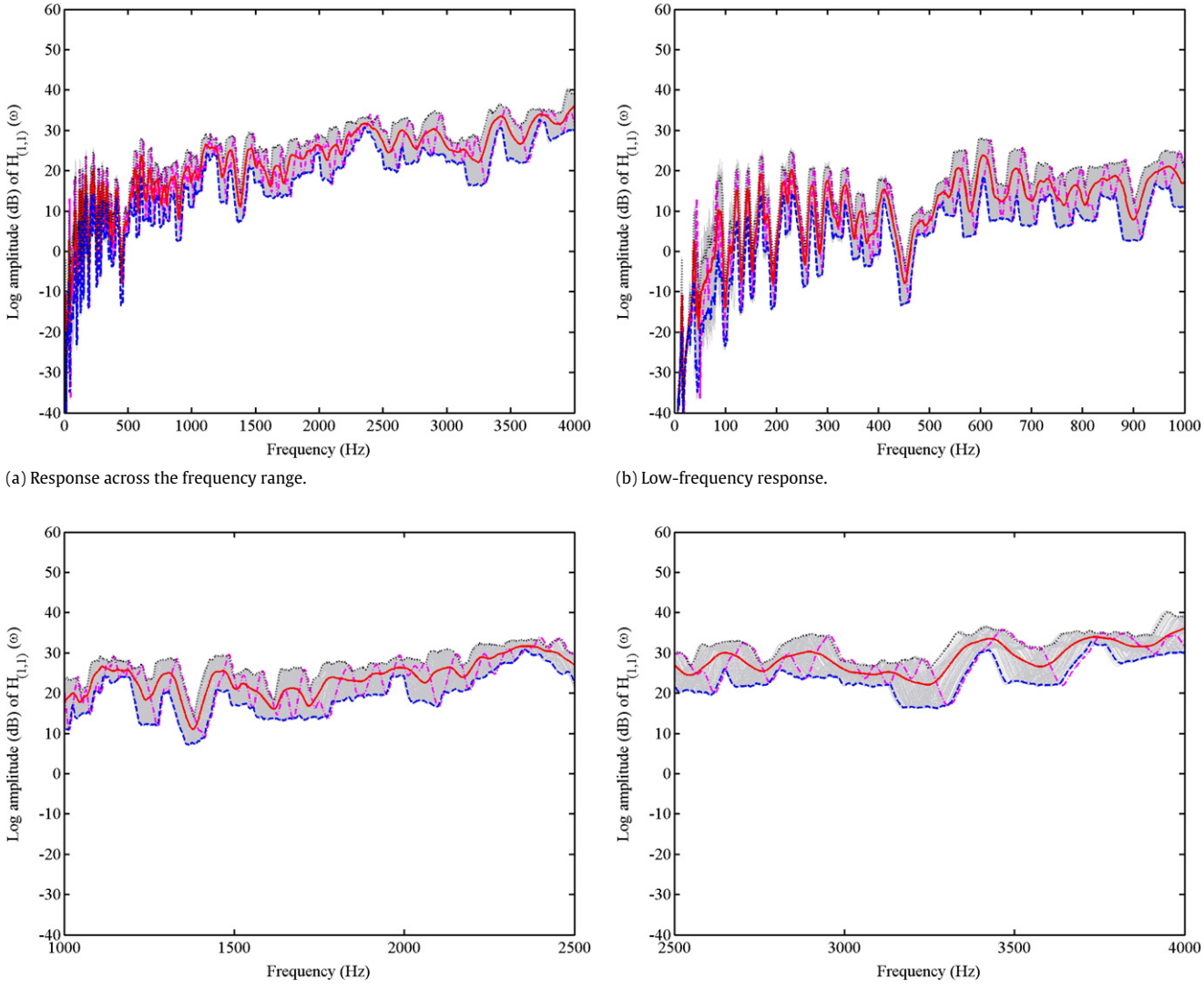

(a) Response across the frequency range.

(b) Low-frequency response.

(c) Medium-frequency response.

(d) High-frequency response.

Fig. 24. Numerically calculated amplitude of the driving-point FRF of the plate at point 1 (nodal coordinate: (4, 6)) with 10 randomly placed oscillators. 100 random FRFs, together with the FRF of the baseline system (- -) ensemble mean (-), 5% (-.-) and 95% (...) probability lines are shown.

boundaries are selected on the basis of the qualitative nature of the response and devised purely for the presentation of the results. The experimental approach discussed here is independent on these selections. The measured FRF data up to 4.0 kHz as shown here is significantly noise-free, since the hard steel tip used was able to excite the whole frequency range. The experimental data shown throughout the paper is the 'raw data' (that is, without any filtering) obtained directly from the LMS system. The ensemble mean follows the result of the baseline system closely except in the low frequency range. The relative variance of the amplitude of the FRF remains more or less constant in the mid- and high-frequency ranges. Equivalent results for the cross FRF at point 2 (see Table 5 for the locations) are shown in Fig. 20.

The general trend of the results is similar to that of point 1 except that the response variability is slightly greater. Note that most of the variability in the FRFs is concentrated at the low-frequency region. This is because the frequency of the attached oscillators are below 70 Hz.

3.4. Numerical simulation

In this section we numerically simulate the experimental system discussed in Section 3.1. The objective here is to determine whether the pattern of uncertainty in the response observed in the experimental data can be observed using the standard Monte Carlo simulation approach often used in probabilistic mechanics. A steel cantilever plate with homogeneous geometric (i.e. uniform thickness) and constitutive properties (i.e. uniform Young's modulus and Poisson's ratio) was considered. The numerical values of the material properties are given in Table 3. This uniform plate simulates the *baseline* system shown in Fig. 13. The diagram of the plate together with the numerical values assumed for the system parameters is shown in Fig. 21. The plate is excited by an unit harmonic force and the responses are calculated at the points shown in the diagram.

The input node corresponds to the location of the shaker shown in Fig. 17 and the output nodes correspond to the locations of the accelerometers shown in Fig. 18. The baseline model is perturbed by a set of spring-mass oscillators, each having natural frequency according to Table 4 and attached at random locations on the plate. The one hundred sets of coordinates of the ten oscillators employed in the experiment are again used here.

The equation of motion of the undamped plate with discrete fixed masses and randomly placed oscillators can be expressed as

$$D\nabla^4 w(x,y,t) + \rho t_h \ddot{w}(x,y,t) + \sum_{j=1}^{6} m_a \ddot{w}(x_{a_j}, y_{a_j}, t)$$

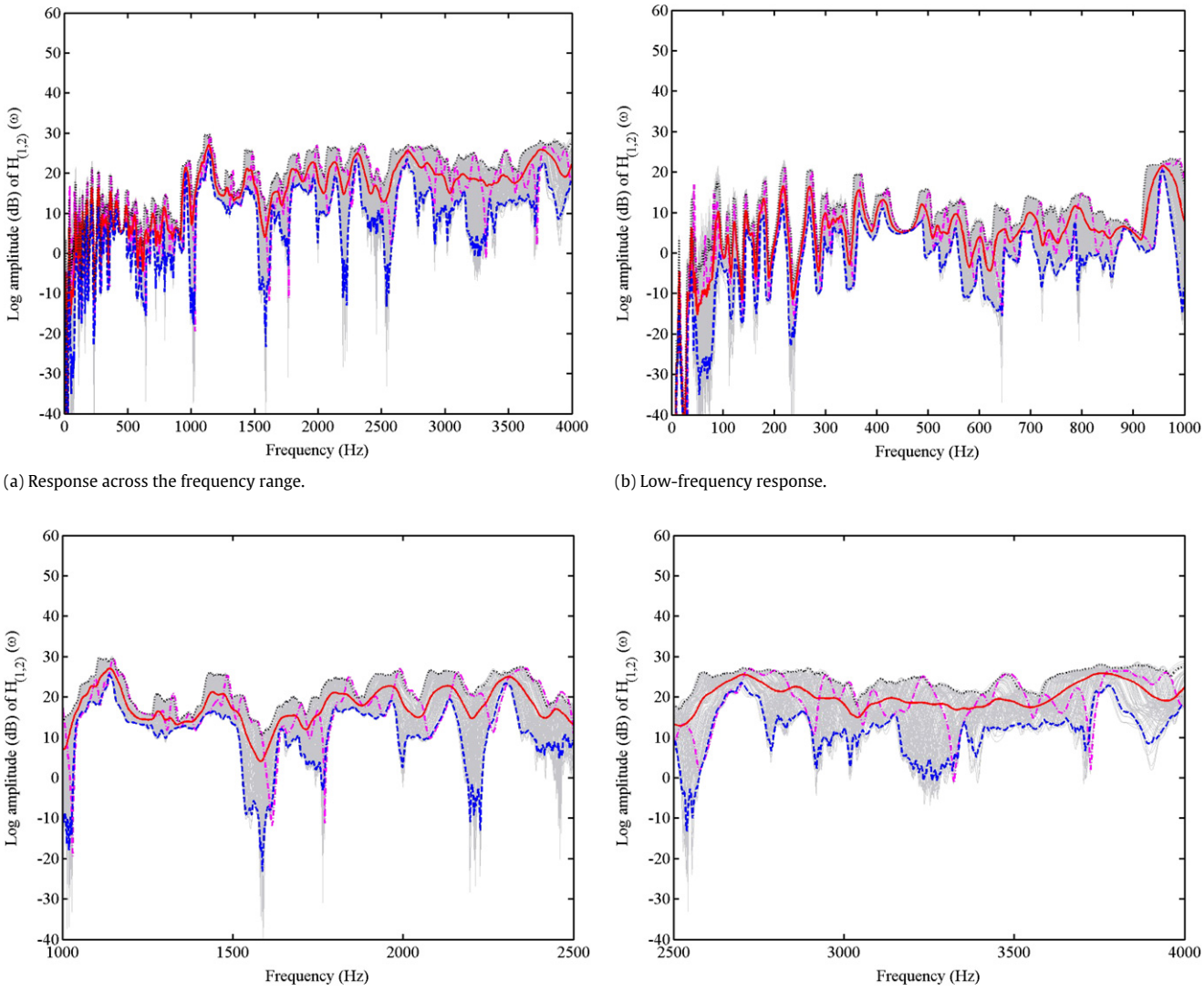

(a) Response across the frequency range.

(b) Low-frequency response.

(c) Medium-frequency response.

(d) High-frequency response.

Fig. 25. Numerically calculated amplitude of the cross-FRF of the plate at point 2 (nodal coordinate: (6, 11)) with 10 randomly placed oscillators. 100 random FRFs, together with the FRF of the baseline system (- -) ensemble mean (-), 5% (-.-) and 95% (...) probability lines are shown.

$$+\sum_{j=1}^{10} m_f \ddot{w}(x_{r_j}, y_{r_j}, t) + \sum_{j=1}^{10} k_{r_j}(w(x_{r_j}, y_{r_j}, t) - z_j(t)) = f(x, y, t) \tag{10}$$

where $\nabla^4 = \left(\frac{\partial}{\partial x^2} + \frac{\partial}{\partial x^2}\right)^2$ is the bi-harmonic differential operator, $D = \frac{Et_h^3}{12(1-\mu^2)}$, m_f is the mass of the magnets and k_{r_j} are the stiffness of the oscillators shown in Table 4. The equations of the oscillators can be expressed as

$$m_r(\ddot{z}_j(t) + g) = k_{r_j}(w(x_{r_j}, y_{r_j}, t) - z_j(t)) \tag{11}$$

where $z_j(t)$ denotes the degree of freedom of the jth oscillator. The applied force $f(x, y, t)$ is the impulse provided by the shaker and has the similar mathematical form given for the beam experiment. The uncertainty in Eq. (10) arises from the randomness in the values of x_{r_j} and y_{r_j}. The damping of the system is introduced using the constant modal damping assumption. We have calculated modal densities and modal overlap factors of the baseline system using the finite element approach and analytical expression given by Xie et al. [53]. The modal density ν for the cantilever plate can be obtained as

$$\nu(\omega) = \frac{L_x k_y}{\pi}\sqrt{\frac{\rho t_h}{D}} + \frac{1}{2}\left(\frac{\rho t_h}{D}\right)^{1/4}\left(\frac{L_x + k_y}{\pi}\right)\omega^{-1/2}. \tag{12}$$

The variation of the modal densities obtained from the above equation and finite element method is shown in Fig. 22(a). Assuming a constant modal damping factor ζ, the modal overlap factor of the system can be calculated as

$$\mu(\omega) = \omega\zeta\nu(\omega) = \zeta\omega\frac{L_x k_y}{\pi}\sqrt{\frac{\rho t_h}{D}} + \frac{1}{2}\zeta\left(\frac{\rho t_h}{D}\right)^{1/4}\left(\frac{L_x + k_y}{\pi}\right)\sqrt{\omega}. \tag{13}$$

Using $\zeta = 0.007$, the variation of the modal overlap factors obtained from the above equation and finite element method is shown in Fig. 22(b). This result shows that, approximately the modal overlap factor is below 0.5 in the low-frequency range (0–1.0 kHz), it is below 1.0 in the mid-frequency range (1.0–2.5 kHz) and it is over 1.0 in the high-frequency range (2.5–4.0 kHz) considered. Again we stress that these boundaries are introduced purely for the purpose of presentation of the experimental results.

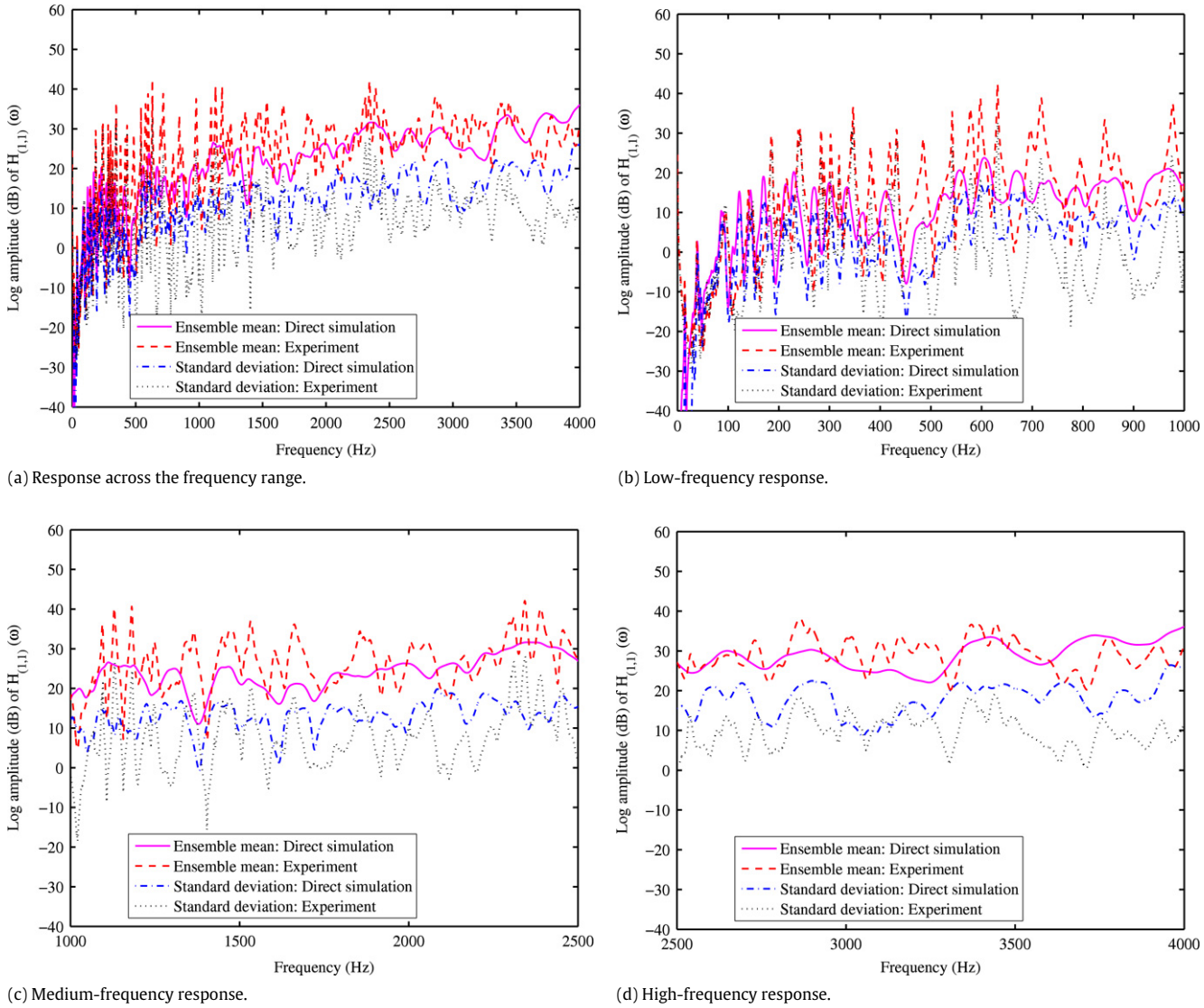

(a) Response across the frequency range.

(b) Low-frequency response.

(c) Medium-frequency response.

(d) High-frequency response.

Fig. 26. Comparison of the mean and standard deviation of the amplitude of the driving-point FRF of the plate at point 1 (nodal coordinate: (4, 6)) with 10 randomly placed oscillators. 100 FRFs, together with the ensemble mean, 5% and 95% probability points are shown.

From Fig. 23 observe that the standard deviations of the natural frequencies are quite small compared to the mean values. The slight variations of the natural frequencies at the lower frequencies correspond to the natural frequencies of the attached oscillators.

The frequency response functions of the system are calculated using the modal superposition and assuming proportional damping as shown in Eq. (9). The first 720 modes are used in the calculation of the frequency response functions. Fig. 23 shows the mean and standard deviation of the natural frequencies of the plate obtained using a Monte Carlo simulation. For the frequency-response function calculation, a modal damping factor of 0.7% is assumed for all of the modes. Fig. 24 shows the amplitude of the frequency response function (FRF) at point 1 (the driving-point FRF, see Table 5 for the location) of the plate without any oscillators (the baseline model). In the same figure 100 samples of the amplitude of the FRF are shown together with the ensemble mean, 5% and 95% probability lines.

In Fig. 24(b)–(d) we have separately shown the low-, medium- and high-frequency response, obtained by zooming around the appropriate frequency ranges in Fig. 24(a). The ensemble mean does not follow the result of the baseline system closely in any frequency range. The relative variance of the amplitude of the FRF remains more or less constant in the mid and high frequency range. Equivalent results for the cross FRF at point 2 (see Table 5 for the locations) are shown in Fig. 25.

The general statistical trend of the results is similar to that for point 1 except that the response variability is slightly higher. Significant variability in the FRFs can be seen at the low-frequency region. This is because the natural frequencies of the 10 attached oscillators at random locations are below 70 Hz.

3.5. Comparisons between numerical and experimental results

It is interesting to compare the experimental results with the Monte Carlo simulations. Fig. 26 compares the ensemble mean and standard deviation of the amplitude of the driving-point frequency response function (FRF) at point 1 obtained from the experiment and Monte Carlo simulation. Fig. 26(b)–(d) show the low-, medium- and high-frequency responses separately, obtained by zooming around the appropriate frequency ranges in Fig. 26(a). The standard deviation of the amplitude of the FRF reaches a peak at the system natural frequencies, which is also predicted by the numerical simulation. Qualitatively the simulation results agree well with the experimental results. The main reason for the

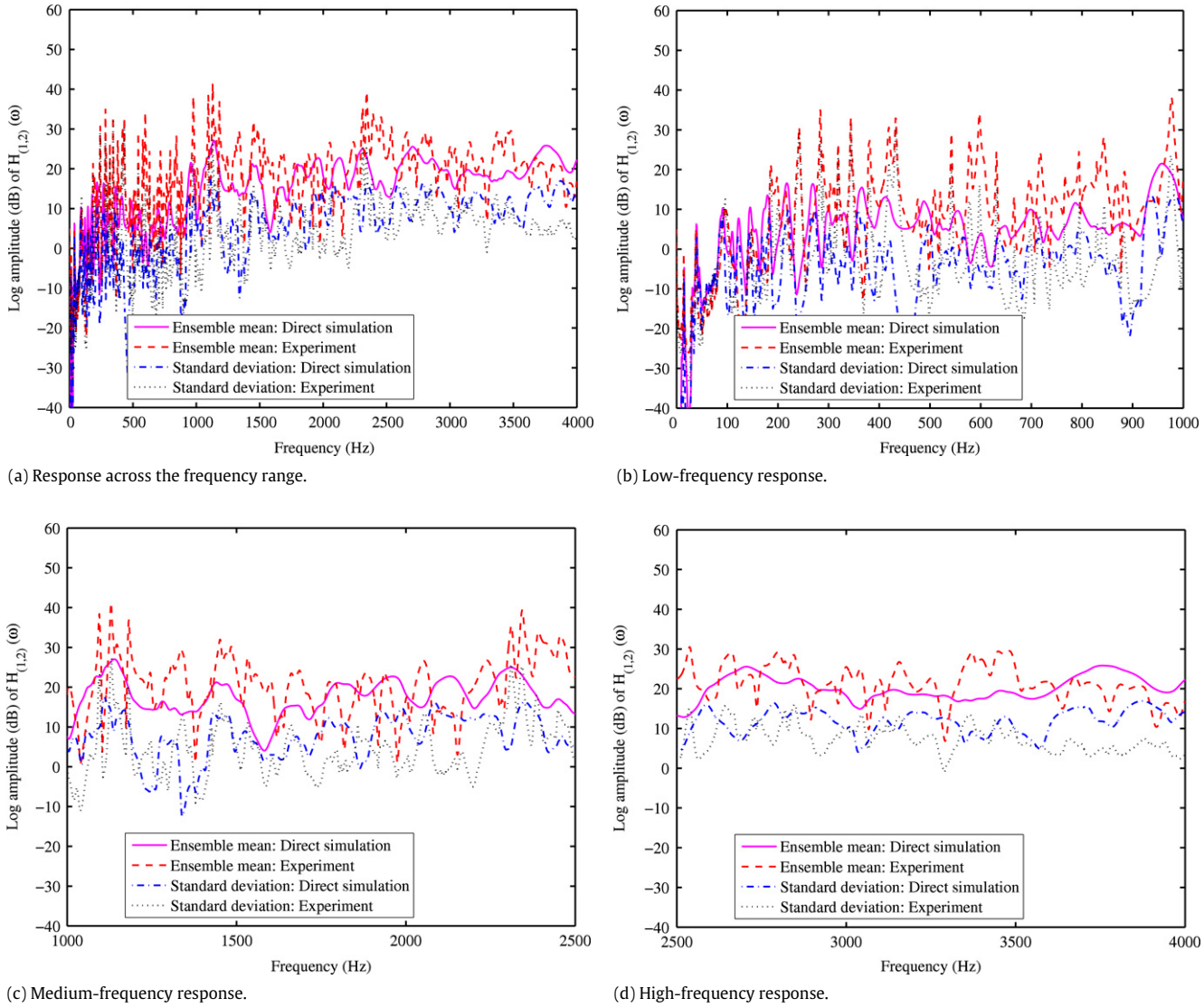

(a) Response across the frequency range.

(b) Low-frequency response.

(c) Medium-frequency response.

(d) High-frequency response.

Fig. 27. Comparison of the mean and standard deviation of the amplitude of the cross-FRF of the plate at point 2 (nodal coordinate: (6,11)) with 10 randomly placed oscillators. 100 FRFs, together with the ensemble mean, 5% and 95% probability points are shown.

discrepancies, especially in the low-frequency regions, is probably due to the incorrect value of the damping factors. In the simulation study a constant damping factor of 0.7% is assumed for all of the modes. Ideally one should measure modal damping factors from experimental measurements for all of the samples and for as many modes as possible and perhaps take an average across the samples for every mode.

Equivalent comparisons for point 2 (a cross FRF) are shown in Fig. 27. For both points, the experimental mean and standard deviation in the low frequency range is quite high compared to numerical results. This can again be attributed to the wrong values of modal damping factors in the analytical model since the pattern of the peaks are strikingly similar but they are separated in 'height'. As in the beam experiment, we have again assumed a constant modal damping factor for all of the modes.

4. Conclusions

This paper has described two experiments that may be used to study methods to quantify uncertainty in the dynamics of structures. The first experiment is about a fixed–fixed beam with 10 randomly placed masses while the second experiment is about a cantilever plate with 10 randomly placed oscillators. One hundred nominally identical beams and plates are created and individually tested using experimental modal analysis. Special measures have been taken so that the uncertainty in the response only arises from the randomness in the mass and oscillator locations and the experiments are repeatable with minimum changes. Such novel measures include:

(a) the use of a shaker as an impact hammer to ensure a consistent force and location for all of the tests,
(b) the use of a ruler to minimize the error in measuring the mass locations in the beam experiment,
(c) the employment of a grid system and nodal points to minimise the error in measuring the oscillator and hammer locations in the plate experiment,
(d) the use of magnets as attached masses for the ease of placement in the beam experiment,
(e) the use of magnets to attach the oscillators in the plate experiment, and
(e) the use of a hard steel tip and a small brass plate on the flexible beam to obtain virtually noise-free data up to 4.5 kHz.

The statistics of the frequency response functions measured at different points are obtained for low-, medium- and high-frequency ranges. More variability in the FRF at the high-frequency range compared to the low-frequency range is observed. This data may be used for the model validation and uncertainty quantification of dynamical systems.

The experimental results are directly compared with a numerical Monte Carlo simulation. A finite element model of a simple Euler–Bernoulli beam and simple thin plate elements are used in the analytical study. The pattern of the response mean and standard deviation obtained in the experimental analysis are predicted using these simple models. The discrepancies between the two approaches are attributed to incorrect values for damping used in the numerical model. This suggests that correct damping values are crucial for the prediction of the response variance of stochastic dynamical systems.

Acknowledgements

SA gratefully acknowledges the financial support of the Engineering and Physical Sciences Research Council through the award of an Advanced Research Fellowship. MIF gratefully acknowledges the support of the Royal Society through a Royal Society-Wolfson Research Merit Award. AS acknowledges the support of a Discovery Grant from Natural Sciences and Engineering Research Council of Canada and the Canada Research Chair Program.

References

[1] Shinozuka M, Yamazaki F. Stochastic finite element analysis: An introduction. In: Ariaratnam ST, Schuëller GI, Elishakoff I, editors. Stochastic structural dynamics: Progress in theory and applications. London: Elsevier Applied Science; 1998.
[2] Ghanem R, Spanos P. Stochastic finite elements: A spectral approach. New York (USA): Springer-Verlag; 1991.
[3] Kleiber M, Hien TD. The stochastic finite element method. Chichester: John Wiley; 1992.
[4] Matthies HG, Brenner CE, Bucher CG, Soares CG. Uncertainties in probabilistic numerical analysis of structures and solids — Stochastic finite elements. Structural Safety 1997;19(3):283–336.
[5] Manohar CS, Adhikari S. Dynamic stiffness of randomly parametered beams. Probabilistic Engineering Mechanics 1998;13(1):39–51.
[6] Manohar CS, Adhikari S. Statistical analysis of vibration energy flow in randomly parametered trusses. Journal of Sound and Vibration 1998;217(1):43–74.
[7] Adhikari S, Manohar CS. Dynamic analysis of framed structures with statistical uncertainties. International Journal for Numerical Methods in Engineering 1999;44(8):1157–78.
[8] Adhikari S, Manohar CS. Transient dynamics of stochastically parametered beams. ASCE Journal of Engineering Mechanics 2000;126(11):1131–40.
[9] Haldar A, Mahadevan S. Reliability assessment using stochastic finite element analysis. New York (USA): John Wiley and Sons; 2000.
[10] Sudret B, Der-Kiureghian A. Stochastic finite element methods and reliability. Tech. rep. UCB/SEMM-2000/08. Berkeley: Department of Civil & Environmental Engineering, University Of California; 2000.
[11] Nair PB, Keane AJ. Stochastic reduced basis methods. AIAA Journal 2002;40(8):1653–64.
[12] Elishakoff I, Ren YJ. Large variation finite element method for stochastic problems. Oxford (UK): Oxford University Press; 2003.
[13] Sachdeva SK, Nair PB, Keane AJ. Comparative study of projection schemes for stochastic finite element analysis. Computer Methods in Applied Mechanics and Engineering 2006;195(19–22):2371–92.
[14] Sachdeva SK, Nair PB, Keane AJ. Hybridization of stochastic reduced basis methods with polynomial chaos expansions. Probabilistic Engineering Mechanics 2006;21(2):182–92.
[15] Hanson KM, Hemez FM. A framework for assessing confidence in computational predictions —- Computational validation series: Part 3. Experimental Techniques 2001;25(4):50–5.
[16] Oberkampf WL, Trucano TG. Verification and validation in computational fluid dynamics. Progress in Aerospace Sciences 2002;38(3):209–72.
[17] Oberkampf WL, Deland SM, Rutherford BM, Diegert KV, Alvin KF. Error and uncertainty in modeling and simulation. Reliability Engineering System Safety 2002;75(3):333–57.
[18] Hemez F.M.. Overview of uncertainty quantification and model verification and validation. In: Pan American advanced study institute (PASI) on damage prognosis. Florianopolis, Brazil; 2003. http://ext.lanl.gov/projects/ei/model_v/pubs/Hemez_03-7640.pdf.
[19] Hemez FM. Uncertainty quantification and the verification and validation of computational models. In: Inman DJ, Farrar CR, Lopes Jr Vicente, Steffen Jr Valder, editors. Damage prognosis for Aerospace, Civil and Mechanical Systems. London, United Kingdom: John Wiley & Sons Ltd; 2004. http://ext.lanl.gov/projects/ei/model_v/pubs/Hemez_03-8491.pdf.
[20] Ferson S, Joslyn CA, Helton JC, Oberkampf WL, Sentz K. Summary from the epistemic uncertainty workshop: Consensus amid diversity. Reliability Engineering System Safety 2004;85(1–3):355–69.
[21] Oberkampf WL, Trucano TG, Hirsch C. Verification, validation, and predictive capability in computational engineering and physics. Applied Mechanics Reviews ASME 2004;57(5):345–84.
[22] Oberkampf WL, Barone MF. Measures of agreement between computation and experiment: Validation metrics. Journal of Computational Physics 2006;217(1):5–36.
[23] Trucano TG, Swiler LP, Igusa T, Oberkampf WL, Pilch M. Calibration, validation, and sensitivity analysis: What's what. Reliability Engineering System Safety 2006;91(10–11):1331–57.
[24] Adhikari S, Woodhouse J. Identification of damping: Part 1 viscous damping. Journal of Sound and Vibration 2001;243(1):43–61.
[25] Adhikari S, Woodhouse J. Identification of damping: Part 2 non-viscous damping. Journal of Sound and Vibration 2001;243(1):63–88.
[26] Soize C. A nonparametric model of random uncertainties for reduced matrix models in structural dynamics. Probabilistic Engineering Mechanics 2000;15(3):277–94.
[27] Soize C. Maximum entropy approach for modeling random uncertainties in transient elastodynamics. Journal of the Acoustical Society of America 2001;109(5):1979–96. Part I.
[28] Soize C. Random matrix theory for modeling uncertainties in computational mechanics. Computer Methods in Applied Mechanics and Engineering 2005;194(12–16):1333–66.
[29] Mignolet MP, Soize C. Nonparametric stochastic modeling of linear systems with prescribed variance of several natural frequencies. Probabilistic Engineering Mechanics 2008;23(2–3):267–78.
[30] Mignolet MP, Soize C. Stochastic reduced order models for uncertain geometrically nonlinear dynamical systems. Computer Methods in Applied Mechanics and Engineering Available online 2008.
[31] Adhikari S. Matrix variate distributions for probabilistic structural mechanics. AIAA Journal 2007;45(7):1748–62.
[32] Adhikari S. Wishart random matrices in probabilistic structural mechanics. ASCE Journal of Engineering Mechanics 2008;134(12):1029–44.
[33] Adhikari S. On the quantification of damping model uncertainty. Journal of Sound and Vibration 2007;305(1–2):153–71.
[34] Adhikari S, Sarkar A. The nature of epistemic uncertainty in linear dynamical systems. In: Proceedings of the 25th international modal analysis conference. IMAC-XXV; 2007.
[35] Lyon RH, Dejong RG. Theory and application of statistical energy analysis. second ed. Boston: Butterworth-Heinmann; 1995.
[36] Keane AJ, Price WG. Statistical energy analysis: An overview with applications in structural dynamics. Cambridge (UK): Cambridge University Press; 1997. First published in Philosophical Transactions of the Royal Society of London, series A. vol. 346. 1994. p. 429–554.
[37] Langley RS. A general derivation of the statistical energy analysis equations for coupled dynamic-systems. Journal of Sound and Vibration 1989;135(3):499–508.
[38] Langley RS, Bremner P. A hybrid method for the vibration analysis of complex structural-acoustic systems. Journal of the Acoustical Society of America 1999;105(3):1657–71.
[39] Sarkar A, Ghanem R. Mid-frequency structural dynamics with parameter uncertainty. Computer Methods in Applied Mechanics and Engineering 2002;191(47–48):5499–513.
[40] Sarkar A, Ghanem R. A substructure approach for the midfrequency vibration of stochastic systems. Journal of the Acoustical Society of America 2003;113(4):1922–34. Part 1.
[41] Ghanem R, Sarkar A. Reduced models for the medium-frequency dynamics of stochastic systems. Journal of the Acoustical Society of America 2003;113(2):834–46.
[42] Langley RS, Cotoni V. Response variance prediction for uncertain vibro-acoustic systems using a hybrid deterministic-statistical method. Journal of the Acoustical Society of America 2007;122(6):3445–63.
[43] Kompella MS, Bernhard BJ. Measurement of the statistical variations of structural-acoustics characteristics of automotive vehicles. In: SAE noise and vibration conference. Warrendale (USA): Society of Automotive Engineers; 1993.
[44] Fahy F. Foundations of engineering acoustics. London, UK: Academic Press Inc.; 2000.
[45] Friswell MI, Coote JA, Terrell MJ, Adhikari S, Fonseca JR, Lieven NAJ. Experimental data for uncertainty quantification. In: Proceedings of the 23rd international modal analysis conference. Orlando (FL, USA): Society of Experimental Mechanics (SEM); 2005.
[46] Ewins DJ. Modal testing: Theory and practice. second ed. Baldock (England): Research Studies Press; 2000.
[47] Maia NMM, Silva JMM, editors. Theoretical and experimental modal analysis. Robetrs JB, editor. Engineering dynamics series, Taunton (England): Research Studies Press; 1997.

[48] J.M.M. Silva, and N.M.M. Maia (Eds.), Modal analysis and testing: Proceedings of the NATO advanced study institute. NATO science series: E: Applied science. Sesimbra, Portugal; 1998.
[49] Géradin M, Rixen D. Mechanical vibrations. second ed. New York (NY): John Wiely & Sons; 1997. Translation of: Théorie des vibrations.
[50] Adhikari S, Friswell MI. Random matrix eigenvalue problems in structural dynamics. International Journal for Numerical Methods in Engineering 2007; 69(3):562–91.
[51] Adhikari S. Joint statistics of natural frequencies of stochastic dynamic systems. Computational Mechanics 2007;40(4):739–52.
[52] Manohar CS, Keane AJ. Statistics of energy flow in one dimentional subsystems. Philosophical Transactions of Royal Society of London 1994;A346: 525–542.
[53] Xie G, Thompson DJ, Jones CJC. Mode count and modal density of structural systems: Relationships with boundary conditions. Journal of Sound and Vibration 2004;274:621–51.